Department of Applied Physics

Making a spin-difference in quantum gases

Miikka Heikkinen

Aalto University

DOCTORAL DISSERTATIONS

Aalto University publication series
DOCTORAL DISSERTATIONS 78/2014

Making a spin-difference in quantum gases

Miikka Heikkinen

A doctoral dissertation completed for the degree of Doctor of Science (Technology) to be defended, with the permission of the Aalto University School of Science, at a public examination held at the lecture hall E (Otakaari 1, Espoo) of the school on 27 June 2014 at 12 o'clock noon.

Aalto University
School of Science
Department of Applied Physics
Quantum Dynamics

Supervising professor
Prof. Päivi Törmä

Thesis advisor
Prof. Päivi Törmä

Preliminary examiners
Prof. Nigel Cooper, University of Cambridge, United Kingdom
Prof. Frank Hekking, Université Joseph Fourier, France

Opponent
Prof. Wilhelm Zwerger, Technische Universität München, Germany

Aalto University publication series
DOCTORAL DISSERTATIONS 78/2014

ISBN 978-952-60-5708-8
ISBN 978-952-60-5709-5 (pdf)
ISSN-L 1799-4934
ISSN 1799-4934 (printed)
ISSN 1799-4942 (pdf)
http://urn.fi/URN:ISBN:978-952-60-5709-5

Unigrafia Oy
Helsinki 2014

Finland

441 697
Printed matter

Aalto University

Abstract

Aalto University, P.O. Box 11000, FI-00076 Aalto www.aalto.fi

Author
Miikka Heikkinen

Name of the doctoral dissertation
Making a spin-difference in quantum gases

Publisher School of Science

Unit Department of Applied Physics

Series Aalto University publication series DOCTORAL DISSERTATIONS 78/2014

Field of research Theoretical and computational physics

Manuscript submitted 7 March 2014 **Date of the defence** 27 June 2014

Permission to publish granted (date) 25 April 2014 **Language** English

☐ **Monograph** ☒ **Article dissertation (summary + original articles)**

Abstract

This thesis studies the theory of quantum gases. We focus on fermionic superfluidity in systems in which the control over the spin degree of freedom has a central role.

We explain the microscopic origin of the spin-asymmetric Josephon effect, and propose methods for realizing this effect experimentally in quantum gases.

We investigate the phenomenon of fermionic superfluidity in the presence of spin-polarization, with our main focus on the Fulde-Ferrel-Larkin-Ovchinnikov (FFLO) phase. We show that the FFLO pairing mechanism leads to an anisotropic speed of sound which can be used to identify the state in experiments. Using real-space dynamical mean field theory (DMFT), we compute the phase diagram of a trapped, spin-polarized Fermi gas in a dimensional crossover from a 1D to a 3D optical lattice. We find that the FFLO state is realized in a broad region of parameters throughout the crossover while the shell structure of the Fermi gas preceding the transition to the full FFLO state shows a strong dependence on the dimensionality. Finally, we utilize the cluster DMFT method to show that the FFLO state is stable against non-local quantum fluctuations even though these fluctuations do affect the critical temperature of the state.

Keywords Quantum gases, Superfluidity, Optical lattice, Hubbard model, Josephson effect, Fulde-Ferrell-Larkin-Ovchinnikov phase, Generalized random-phase approximation, Dynamical mean-field theory

ISBN (printed) 978-952-60-5708-8 **ISBN (pdf)** 978-952-60-5709-5

ISSN-L 1799-4934 **ISSN (printed)** 1799-4934 **ISSN (pdf)** 1799-4942

Location of publisher Helsinki **Location of printing** Helsinki **Year** 2014

Pages 135 **urn** http://urn.fi/URN:ISBN:978-952-60-5709-5

A? Aalto-yliopisto

Tiivistelmä

Aalto-yliopisto, PL 11000, 00076 Aalto www.aalto.fi

Tekijä
Miikka Heikkinen

Väitöskirjan nimi
Spin-asymmetria kvanttikaasuissa

Julkaisija Perustieteiden korkeakoulu

Yksikkö Teknillisen fysiikan laitos

Sarja Aalto University publication series DOCTORAL DISSERTATIONS 78/2014

Tutkimusala Teoreettinen ja laskennallinen fysiikka

Käsikirjoituksen pvm 07.03.2014 **Väitöspäivä** 27.06.2014

Julkaisuluvan myöntämispäivä 25.04.2014 **Kieli** Englanti

☐ **Monografia** ☒ **Yhdistelmäväitöskirja (yhteenveto-osa + erillisartikkelit)**

Tiivistelmä

Tässä väitöskirjassa käsitellään kvanttikaasujen teoriaa painottuen systeemeihin, joissa spin-vapausasteen kontrolloinnilla on keskeinen sija.

Työssä selitetään spin-asymmetrisen Josephsonin ilmiön mikroskooppinen syntymekanismi ja esitetään menetelmiä, joilla kyseistä ilmiötä voidaan tutkia kokeellisesti kvanttikaasujen avulla.

Väitöskirjassa tutkitaan spin-polarisoituneitten fermionisysteemien suprajuoksevuutta erityisenä tarkastelun kohteena Fulde-Ferrell-Larkin-Ovchinnikov -tila (FFLO). Työssä osoitetaan, että FFLO-tila voidaan tunnistaa sen pariutumismekanismista aiheutuvan epäisotrooppisen äänennopeuden perusteella. Työssä sovelletaan dynaamisen keskiarvotetun kentän teoriaa (DMFT) spin-polarisoituneen fermikaasun faasidiagrammin laskentaan harmonisen loukun ja eridimensioisten hilojen tapauksessa. Keskeisenä tuloksena on, että FFLO-tila on olemassa laajalla parametrialueella kvasiyksidimensioisista hiloista kolmidimensioisiin hiloihin, mutta FFLO tilan syntyä edeltävä fermikaasun rakenne riippuu vahvasti systeemin dimensionaalisuudesta. Tämän lisäksi työssä osoitetaan, että FFLO-tila on stabiili ei-lokaalien kvanttifluktuaatioden suhteen klusteri-DMFT-menetelmällä laskettetujen tulosten perusteella, vaikka nämä fluktuaatiot muuttavatkin FFLO-tilan kriittistä lämpötilaa.

Avainsanat Kvanttikaasut, Suprajuoksevuus, Optinen hila, Hubbardin malli, Josephsonin ilmiö, Fulde-Ferrell-Larkin-Ovchinnikov -tila, Yleistetty satunnaisen vaiheen approksimaatio, Dynaamisen keskiarvostetun kentän teoria

ISBN (painettu) 978-952-60-5708-8 **ISBN (pdf)** 978-952-60-5709-5

ISSN-L 1799-4934 **ISSN (painettu)** 1799-4934 **ISSN (pdf)** 1799-4942

Julkaisupaikka Helsinki **Painopaikka** Helsinki **Vuosi** 2014

Sivumäärä 135 **urn** http://urn.fi/URN:ISBN:978-952-60-5709-5

Preface

The research reported in this doctoral thesis was conducted at the Department of Applied Physics and the Centre of Excellence in Computational Nanoscience (COMP), Aalto University School of Science. I am grateful to my supervisor, Professor Päivi Törmä, for offering me a magnificent opportunity to work at the very forefront of science. Her unparalleled vision and tremendous support have been invaluable for the accomplishment of this thesis.

I would sincerely like to thank Dr. Francesco Massel, Dr. Jussi Kajala, Dr. Mikko Leskinen, Dr. Sorin Paraoanu, Dr. Dong-Hee Kim, Mr. Juha Kreula, and Prof. Matthias Troyer, with whom it has been my pleasure and my privilege to collaborate during my doctoral studies. Furthermore, I am greatly indebted to Dr. Kim for being my guide to the world of dynamical mean-field theory and to Prof. Troyer for inviting me for a wonderful research visit at ETH Zürich.

I have been very fortunate to always enjoy an excellent working atmosphere created by colleagues who passionately engage in inspiring discussions about physics, who kindly help out a friend in need, and who perhaps even take part in a relaxing (albeit sometimes death-defying) game of futsal or frisbee golf. I would like to thank all of these outstanding people, in particular Dr. Jami Kinnunen, Dr. Jani-Petri Martikainen, Mr. Tuomas Vanhala, Dr. Timo Koponen, Mr. Olli Nummi, Dr. Antti-Pekka Eskelinen, Dr. Tommi Hakala, Dr. Jildou Baarsma, Mr. Heikki Rekola, Ms. Anne-Maria Visuri, Ms. Anna Korolyuk, Mr. Elmer Doggen, Dr. Tuomas Lahtinen and Mr. Kévin Franke.

Throughout my studies, I have been happy to share the company of so many bright and brilliant people. It is here that I simply have to mention Dr. Jaakko Nieminen, Dr. Markus Ojala, Mr. Veli Peltola, and Dr. Niko Vuokko, who have all been a real source of inspiration to me, and from

whom I have learned a great deal. I would also like to take the opportunity to acknowledge the important work of every teacher I have had starting from the lecturers of the various summer schools I have participated in, going through the ranks of Aalto University as well as the coaching staff of the Finnish International Mathematical Olympiad team, all the way back to the incredibly supportive and encouraging educators of my home town, Sotkamo.

All of my friends and my family deserve my humblest thanks for their continuous support. I dedicate this thesis to my dearest Elina – Thank you for always being there for me.

I gratefully acknowledge the financial support offered by the Finnish Doctoral Programme in Computational Sciences (FICS), Aalto researcher training scholarship programme, and the KAUTE foundation, as well as the computational resources provided by CSC – IT Center for Science.

Helsinki, May 22, 2014,

Miikka Heikkinen

Contents

List of Publications

This thesis consists of an overview and of the following publications which are referred to in the text by their Roman numerals.

I M. O. J. Heikkinen, F. Massel, J. Kajala, M. J. Leskinen, G. S. Paraoanu, and P. Törmä. Spin-Asymmetric Josephson Effect. *Physical Review Letters*, 105, 22, 225301, Nov 2010.

II M. O. J. Heikkinen and P. Törmä. Collective modes and the speed of sound in the Fulde-Ferrell-Larkin-Ovchinnikov state. *Physical Review A*, 83, 5, 053630, May 2011.

III M. O. J. Heikkinen, D.-H. Kim and P. Törmä. Finite temperature stability and dimensional crossover of exotic superfluidity in lattices. *Physical Review B*, 87, 22, 224513, June 2013.

IV J. M. Kreula, M. O. J. Heikkinen, F. Massel and P. Törmä. Tunable critical supercurrent and spin-asymmetric Josephson effect in superlattices. *Physical Review B*, 89, 6, 064502, Feb 2014.

V M. O. J. Heikkinen, D.-H. Kim, M. Troyer and P. Törmä. Non-local quantum fluctuations and fermionic superfluidity in the attractive Hubbard model. Submitted to *Physical Review Letters*, 27 Feb 2014, arXiv:1402.6939.

Author's Contribution

Publication I: "Spin-Asymmetric Josephson Effect"

The author carried out the linear response calculations and contributed to formulating the physical interpretation of the results. The author wrote a significant part of the manuscript text.

Publication II: "Collective modes and the speed of sound in the Fulde-Ferrell-Larkin-Ovchinnikov state"

The author carried out the analytical and numerical calculations and was the main writer of the the manuscript text.

Publication III: "Finite temperature stability and dimensional crossover of exotic superfluidity in lattices"

The author implemented the computational methods and carried out the numerical calculations. The author was the main writer of the the manuscript text.

Publication IV: "Tunable critical supercurrent and spin-asymmetric Josephson effect in superlattices"

The author studied the connection of the spin-asymmetric Josephson effect to solid-state systems and carried out the related analytical derivations. The author contributed to the analysis of the numerical results. The author wrote a major part of the manuscript text.

Publication V: "Non-local quantum fluctuations and fermionic superfluidity in the attractive Hubbard model"

The author implemented the computational methods and carried out the numerical calculations. The author was the main writer of the manuscript text.

1. Quantum gases

Condensed matter physics presents us with an almost insurmountable computational challenge. Even with the massive computational resources of today, it remains an active research topic to solve efficiently *approximate* theoretical models, laid out to capture only the most essential qualitative features of the full quantum many-body problem.

In recent years, quantum gases have emerged as a promising testbed of condensed matter theory [1, 2, 3]. At temperatures bordering absolute zero, in the nanokelvin regime, the same quantum laws which operate in condensed matter systems become manifest in a gas of atoms. The crucial advantage that the experiments on atoms have is that the atomic systems can be controlled very systematically, e.g. their interaction strength can be tuned on a continuous scale from strongly attractive to strongly repulsive [4]. Even more so, the quantum gas systems can be tailored to realize to a high precision physical models, which in condensed matter systems are only crude approximations, such as the Hubbard model [5]. Thus, the experiments with quantum gases can for instance address the question of whether a particular phenomenon we observe in solid state systems can be realized within the confinements of a given model or not. From another point of view, computational results can be compared directly against experiment, laying a basis for benchmarking and developing further these methods. Finally, the vast array of experimental possibilities invites us to attempt engineering completely new quantum many-body phenomena. These aspects make quantum gases one of the most interesting venues of science today.

In the following sections, we introduce the concept of quantum gases and explore the conditions under which these system are realized, starting from a discussion about the spin-statistics of composite particles.

1.1 Spin-statistics of composite particles

One of the most interesting features of quantum mechanics is that it is not just a more accurate formulation of the laws of motion of Newtonian mechanics. In the quantum realm, a completely new principle enters our description of nature in the form of a symmetry constraint for identical particles. Furthermore, the precise form of this symmetry constraint is connected to the intrinsic angular momentum, the spin, of the particles. This principle is known as the spin-statistics theorem [6]. Fundamentally, the spin-statistics theorem describes only elementary particles, but it can be extended to composite particles such as atoms to an often excellent approximation. From the the theoretical point of view, this suggests that fundamental implications of spin-statistics are important and can be observed in systems of composite particles.

The spin-statistics theorem states that in a space-time with three space-like and one time-like dimension only two kinds of elementary particles, bosons and fermions, can exist. Particles with integer spin are bosons. A field describing identical bosons obeys the following equal-time commutation relations

$$\left[\psi_\sigma(\mathbf{r}), \psi_{\sigma'}(\mathbf{r}')\right] = 0, \tag{1.1}$$

$$\left[\psi^\dagger_\sigma(\mathbf{r}), \psi^\dagger_{\sigma'}(\mathbf{r}')\right] = 0, \tag{1.2}$$

$$\left[\psi_\sigma(\mathbf{r}), \psi^\dagger_{\sigma'}(\mathbf{r}')\right] = \delta_{\sigma\sigma'}\delta(\mathbf{r}-\mathbf{r}'). \tag{1.3}$$

Particles with half-integer spin are fermions. A field of identical fermions obeys the anticommutation relations given by

$$\left\{\psi_\sigma(\mathbf{r}), \psi_{\sigma'}(\mathbf{r}')\right\} = 0, \tag{1.4}$$

$$\left\{\psi^\dagger_\sigma(\mathbf{r}), \psi^\dagger_{\sigma'}(\mathbf{r}')\right\} = 0, \tag{1.5}$$

$$\left\{\psi_\sigma(\mathbf{r}), \psi^\dagger_{\sigma'}(\mathbf{r}')\right\} = \delta_{\sigma\sigma'}\delta(\mathbf{r}-\mathbf{r}'). \tag{1.6}$$

Here, the commutator of operators A and B is defined as $[A,B] = AB - BA$, and the anticommutator as $\{A,B\} = AB + BA$. The operator $\psi_\sigma(\mathbf{r})$ ($\psi^\dagger_\sigma(\mathbf{r})$) annihilates (creates) a particle at the spin state σ and the position $\mathbf{r}$. The commutation relations above include the information that the wave function of identical bosons is symmetric under the exchange of two particles and similarly that the wave function of identical fermions is antisymmetric. The antisymmetry-property of Fermions leads to the renowned Pauli exclusion principle, which states that two identical fermions cannot occupy the same quantum state [7].

Regarding composite particles, in many applications it is well-justified to assume that a particle consisting of an odd number of elementary fermions and any number of elementary bosons is a fermion, while a composite of an even number of fermions and any number of bosons is a boson. To illustrate the nature of this approximation, we consider the spin-statistics theorem in the case of a composite of two fermions.

Following reference [8], we begin by defining the composite particle as a bound state of the two elementary fermions with the creation operator $\Psi^\dagger(\mathbf{R})$ defined as

$$\Psi^\dagger(\mathbf{R}) = \int d\mathbf{r}\phi(\mathbf{r})\psi_1^\dagger(\mathbf{R}+\mathbf{r}/2)\psi_2^\dagger(\mathbf{R}-\mathbf{r}/2), \tag{1.7}$$

where $\mathbf{R}$ is the center of mass coordinate of the system, $\mathbf{r}$ is the relative coordinate between the two constituents, and $\phi(\mathbf{r})$ is the wave-function of the bound state.

The commutation relations of the composite field at positions $\mathbf{R}$ and $\mathbf{R}'$ can then be derived from the commutation relations of the elementary fermions. For two annihilation operators and for two creation operators we find the same form as for elementary particles

$$\left[\Psi(\mathbf{R}), \Psi(\mathbf{R}')\right] = 0, \tag{1.8}$$

$$\left[\Psi^\dagger(\mathbf{R}), \Psi^\dagger(\mathbf{R}')\right] = 0. \tag{1.9}$$

The relations above imply that the wave function of a system of an arbitrary number of these composites is always symmetric. However, the commutation relation between the creation and annihilation operator does not reduce to the delta-function as it does with the elementary particles. Instead, we obtain

$$\begin{aligned}\left[\Psi(\mathbf{R}), \Psi(\mathbf{R}')^\dagger\right] &= \delta(\mathbf{R}-\mathbf{R}') \\ &- 2\int d\mathbf{r}\phi(\mathbf{r})\phi^*(\mathbf{r}+2(\mathbf{R}-\mathbf{R}'))\psi_1^\dagger(\mathbf{R}'+\mathbf{r}/2)\psi_1(\mathbf{R}'+\mathbf{r}/2+2(\mathbf{R}-\mathbf{R}')) \\ &- 2\int d\mathbf{r}\phi(\mathbf{r})\phi^*(\mathbf{r}-2(\mathbf{R}-\mathbf{R}'))\psi_2^\dagger(\mathbf{R}'-\mathbf{r}/2)\psi_2(\mathbf{R}'-\mathbf{r}/2+2(\mathbf{R}-\mathbf{R}')).\end{aligned} \tag{1.10}$$

The expression above is sufficient to make the point that the commutation relations of composite particles are modified with respect to those of elementary particles. In order to gain some more insight into when the correction term above can safely be neglected, we compute the expected value of the equation above for a many-body state $|\chi\rangle$ with a homogeneous number density n for the composites, which is the same as the number

density of each component. In doing so, we assume that the wave function ϕ is sufficiently localized to approximate the matrix elements of the remaining operators with the density. Finally, we integrate the result over the coordinate $\mathbf{R}'$ in order to have a meaningful comparison with the delta-function and the correction term. We obtain

$$\int d\mathbf{R}' \, \langle\chi| \left[\Psi(\mathbf{R}), \Psi^\dagger(\mathbf{R}')\right] |\chi\rangle = 1 - 2\alpha r_0^3 n. \tag{1.11}$$

Here r_0 is the effective radius of the composite particle and α is dimensionless factor on the order of one, remaining from the overlap integral. For elementary particles the integral above is equal to unity, and this result is recovered if the total volume taken by all the composites is small in comparison to the volume of the system, $nr_0^3 \ll 1$. In other words, the composite particles can be regarded as bosons if the system is dilute.

The treatment above generalizes to composites of an arbitrary number of fermions and bosons. The expressions for the (anti)commutation relations contain more correction terms for larger composites, but the main observation remains the same. A rather important assumption embedded in the calculation is that it is valid only if the bound state ϕ remains well-defined in the dynamical evolution of the system, i.e. that the composite state is reasonable from the point of view of energetics. For instance, were two composites to collide so strongly that a chemical reaction occurs, the description in terms of composite particles as defined in Equation (1.7) would be insufficient to begin with.

To illustrate the criterion on the diluteness, consider for example that the number density of air is roughly $n = 2.5 \times 10^{19} \frac{1}{\mathrm{cm}^3}$ while the radius of a nitrogen molecule is on the order of $r_0 = 1.5 \times 10^{-10} m$ yielding $r_0^3 n \approx 8 \times 10^{-5} \ll 1$. Thus, air can be safely regarded as a collection of elementary particles from the point of view of quantum statistics. However, it is perfectly obvious that the quantum statistical effects are completely absent in the air surrounding us, and air can in fact be regarded a classical gas to an excellent approximation. In the following section, we examine more thoroughly the conditions under which the exploration of the exiting world of quantum statistics is possible and introduce the concept of quantum gases.

1.2 Reaching the quantum statistical regime

Quantum gases are vapors of atoms or molecules for which the effects of quantum statistics are important – not only to account for the internal structure of the constituents, but also to describe their collective behavior. In the following, we explore under what conditions, and by which means, such a requirement can be met.

A simple criterion for observing quantum statistical effects can be deduced from the de Broglie wavelength $\lambda = h/p$, where h is the Planck constant and p the momentum. At interparticle distances below or comparable to λ one would expect quantum mechanical effects to be significant. If the particles in question are also free to move about and change their positions, as in a gas, one would expect for the symmetry properties to place restrictions on identical particles, and thus, to bring about the effects of quantum statistics. We may also anticipate that quantum statistics prevails at low momenta, or energies. Therefore, in thermal equilibrium, we should expect to run into quantum statistics at low temperatures. A somewhat more quantitative criterion is obtained by comparing the average wavelength at a given temperature, i.e. the thermal de Broglie wavelength defined as

$$\lambda_T = \frac{h}{\sqrt{2\pi m k_b T}}, \tag{1.12}$$

to the average distance between particles

$$d = n^{-1/3}. \tag{1.13}$$

In the equations above, m is the mass of the particles, k_b the Boltzmann constant, T the temperature and n the number density. We thus arrive at the following criterion for the appearance of quantum statistical effects:

$$d \leq \lambda_T \quad \text{or} \quad k_b T \leq \frac{h^2 n^{2/3}}{2\pi m}. \tag{1.14}$$

The criterion above turns out to be extremely demanding for any gas made of atoms or molecules. Partly, the reason is simply that the large mass of individual atoms or molecules amounts to a miniscule thermal de Broglie wavelength in comparison to, say, electrons. More importantly, the density of the gas in any experimental setup is very low, setting a very stringent criterion for the temperature. Here, it needs to be pointed out that at low temperatures a gas has a strong tendency to form a solid, and in fact, the gaseous phase can only exist as a metastable state of

the system in the quantum statistical regime. Now, the formation of the solid requires three-body collisions to occur in the gas, and these collisions become more likely with increasing density. Thus, the lifetime of the metastable gas becomes the longer the more dilute the gas is – from this point of view, the diluteness of the system is a desirable property. On a further note, the suppression of three-body processes because of diluteness implies that in the theoretical description of quantum gases it is typically sufficient to consider two-body interactions.

In experiments, the temperature of a quantum gas is typically well below $1\ \mu\mathrm{K}$, while the density would be somewhere in the vicinity of $10^{12} - 10^{15} \frac{1}{cm^3}$. For instance for $^6\mathrm{Li}$ we have $\lambda_T \approx 0.7\ \mu\mathrm{m}$ at the temperature of $T = 1\ \mu\mathrm{K}$, while an average density of $n = 10^{14} \frac{1}{cm^3}$ would yield an interparticle distance of $d = 0.2\ \mu\mathrm{m}$. The criterion for using the spin-statistics of elemetary particles to atoms in such conditions is fullfilled by a wide margin – for instance with the atomic radius of lithium, $r_0 = 150\ \mathrm{pm}$, we have $r_0^3 n \approx 3 \times 10^{-10} \ll 1$. However, it is noteworthy that while the atoms can be regarded as elementary particles from the point of view of quantum statistics, the atoms' internal structure, in addition to providing a pseudo-spin, offers the basis for e.g. confining them and controlling their interactions. The usefulness of quantum gases as quantum testbeds of condensed matter systems largely originates from this fact.

Reaching the extreme conditions quoted above is a magnificent feat which has required the systematic effort of developing and combining several completely new ways of manipulating atomic gases. Present day quantum gas setups utilize magneto-optical trapping [9] and all-optical trapping [10] to confine the system at different stages of the experiment, while the most common cooling techniques consist of laser-cooling through Doppler and Sisyphus mechanisms [11] and evaporative cooling [12]. The cooling of fermionic systems contains additional difficulties in comparison to bosons. The evaporative cooling requires the repeated thermalization of the gas by two-body collisions. However, at low temperatures the two-body scattering occurs predominantly through the s-partial wave channel, which is not allowed for identical fermions because of its even symmetry. Therefore, fermions have to be cooled either as multi-spin systems or by means of symphatetic cooling through collisions with another, more easily cooled gas [13]. In the multi-spin (or usually two-spin) experiments of a single atomic isotope, the relative occupation of each spin-state after the cooling process can be controlled very precisely by driving transitions be-

tween these states with radio-frequency pulses [14, 15]. This technique is a key motivation behind Publication II, Publication III and Publication V which study exotic superfluidity in spin-population imbalanced Fermi gases.

The first true demonstration of the experimental capabilities of quantum gases took place in 1995 with the achievement of Bose-Einstein condensation (BEC) [16, 17, 18]. Subsequent experiments on Bose gases demonstrated e.g. the macroscopic interference between two BECs [19] and the superfluidity of a BEC [20, 21]. The first degenerate Fermi gas, in turn, was prepared successfully in 1999 [22]. This was followed by a series of experiments on two-component Fermi gases, which led to the observation of Fermion pairing and superfluidity [23, 24, 25, 26, 27, 28, 29]. Of particular relevance to this thesis are the realization of superfluidity in the presence of spin-population imbalance [14, 15], and moreover, the advances in experimental techniques with mass-imbalanced Fermi gases, i.e. systems where the pseudo spin states correspond to different atomic isotopes or elements [30, 31, 32, 33]. The examples listed here constitute only a small fraction of the experimental work on quantum gases. Thus far, we have in fact neglected an arrangement central to this thesis, and more generally, to the task of constructing an experimental testbed for condensed matter theory. The arrangement in question is of course the optical lattice. We shall examine optical lattices more closely in the following chapter.

2. Fermionic atoms in optical lattices

An optical lattice is a periodic potential acting on atoms and created by the interference pattern of laser beams. It is the quantum gas counterpart of the crystal lattice of a solid, with the notable difference that the typical optical lattice does not have lattice defects or phonon excitations.

One of the hallmark achievements of quantum gases is the experimental realization of the Hubbard model in optical lattices to an unprecedented accuracy. This feat is a prime example of quantum gases offering an interface between theory and experiment, in this case for studying the physics of the Hubbard model as well as for the development and benchmarking of new computational methods for lattice problems. Here, the first major breakthrough was the realization of the superfluid-Mott transition of a Bose gas [34, 35, 36]. More recently, the Mott transition has been observed for fermionic systems as well [37, 38]. Other achievements include the imaging of Fermi surfaces [39], single site resolved imaging [40, 41] and the realization of the Dicke quantum phase transition [42]. At the moment, the experiments are progressing towards the study of quantum magnetism [43] and fermionic superfluidity in lattices.

In the following, we first introduce the concept of optical lattices and then proceed with the Hubbard model. As the discussion involves mainly single particle properties, it is to a large extent applicable to both bosons and fermions. The main difference between the two statistics in this chapter is in the form of the on-site interaction term of the Hubbard model. For fermions, there is no local interaction between the same spin components because of the Pauli exclusion principle, whereas for bosons, interaction between all spin components would be allowed.

2.1 Optical lattices

The optical lattice potential arises via the AC Stark effect, in which a time-varying electric field polarizes the atom, while at the same time interacting with this induced polarization and thus changing the energy of the atom locally. Optical dipole traps are based on the same effect [13]. For typical electric field strengths, the effect can be described using second order perturbation theory, and because of the fast oscillation of the electric field the temporal average of the resulting potential can be used instead of the time-dependent potential itself.

The simplest scenario is the one-dimensional optical lattice created by the standing wave of two counter-propagating laser beams with frequency ω_L and wave-vector k_L. Assuming that the lasers couple significantly only to a single optical transition of the atom with frequency ω_0, the atom can be treated in a two level approximation. With these assumptions the time-averaged second order Stark shift of the ground state energy of the atom, i.e. the optical potential, can be written as

$$V_L(\mathbf{r}) = \frac{\omega_L}{2\epsilon_0} \frac{|\langle e|\,\mathbf{d}\,|g\rangle|^2}{\omega_L - \omega_0} I(\mathbf{r}). \tag{2.1}$$

Here ϵ_0 is the permittivity of vacuum, and $\langle e|\,\mathbf{d}\,|g\rangle$ is the matrix element of the dipole operator $\mathbf{d} = -e\hat{\mathbf{r}}$ between the ground state $|g\rangle$ and the excited state $|e\rangle$ of the atom. The laser intensity is given by $I(\mathbf{r}) = \frac{1}{2}c\epsilon_0|\mathbf{E}(\mathbf{r})|^2$ where c is the speed of light and $\mathbf{E}(\mathbf{r})$ the electric field strength. Notice that the optical potential can either repel or attract the atoms depending on the detuning of the laser with respect to the transition frequency. For blue detuned lasers ($\omega_L > \omega_0$) the optical potential is repulsive and the atoms are pushed towards the minima of the intensity, while conversely, for red detuned lasers ($\omega_L < \omega_0$) the atoms are drawn to the intensity maxima.

Now, for a standing wave, we may rewrite the intensity as $I(\mathbf{r}) = I_0 \sin^2(\mathbf{k}_L \cdot \mathbf{r})$ with I_0 the maximum intensity. Finally, upon defining

$$V_0 = \frac{\omega_L}{2\epsilon_0} \frac{|\langle e|\,\mathbf{d}\,|g\rangle|^2}{\omega_L - \omega_0} I_0, \tag{2.2}$$

we have

$$V_L(\mathbf{r}) = V_0 \sin^2(\mathbf{k}_L \cdot \mathbf{r}). \tag{2.3}$$

Since the counterpropagating lasers form a standing wave, the lattice constant a is half of the laser wavelength, $a = 1/(2k_L) = \lambda_L/2$. With two

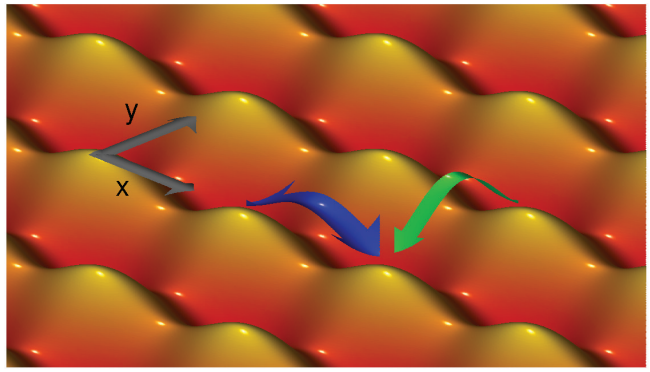

Figure 2.1. The potential landscape of a 2D square optical lattice. Here, the intensity of the standing laser wave along the y-axis is twice as strong as of that along the x-axis. In the resulting lattice, the tunneling of atoms from one lattice site to another is substantially easier along the x-axis (blue arrow) than the y-axis (green arrow). The possibility to have optical lattices of such intermediate dimensionality motivated the studies on the 1D-3D dimensional crossover reported in Publication III and Publication V.

counterpropagating lasers, say directed along the x-axis, the system is still translation invariant in the y- and z-directions.[1] If a pair of counterpropagating laser beams is added also along the y- and z-directions, a cubic lattice is formed. While the majority of the pioneering experiments in optical lattices have been carried out in rectangular geometries [5], the variety of lattices has increased recently to include for example triangular and hexagonal lattices [44, 45]. In addition to this, a technique based on holographic masks holds promises for creating arbitrary two-dimensional optical potentials [40].

Typically, the lattice depth V_0 is given in the units of the recoil energy $E_R = \hbar^2 k_L^2/2m$, where m is the mass of the atom. The lattice depth can be tuned very flexibly through the laser intensity I_0, and in typical experimental setups V_0 is in the range of $V_0 = 1E_R \ldots 30E_R$. In the following section on the Hubbard model, we will examine in more detail the different regimes of the lattice depth.

On a final note, the versatility of optical lattices is not restricted only to creating static geometries. Quite the contrary, the lattice itself can be utilized in several ways to actively probe and manipulate the many-body

[1] The terminology here is somewhat ambiguous, as this configuration is indeed known as a 1D optical lattice. If strong confinement is introduced in the y- and z-directions a lattice with effectively only one spatial dimension is formed. This is also called a 1D optical lattice.

system [46]. To give some examples of this, varying the lattice intensity can be exploited in the form of lattice modulation spectroscopy [47], and lattice configurations which allow the merging of adjacent lattice sites facilitate the measurement of non-local correlations [48]. The flexibility of optical lattices is an essential ingredient also in Publication IV of this thesis in the form of offering a possibility to switch on a spin-dependent superlattice.

2.2 Hubbard model

The Hubbard model is arguably the simplest possible model to describe interacting quantum mechanical particles on a lattice. It consists of a single energy band occupied by particles which can interact with other particles on the same lattice site and tunnel between neighboring lattice sites [49, 50]. This is the simplest possible improvement of the tight binding model to include an interaction between particles. The Hubbard model was originally conceived to describe materials with localized electrons on the outermost band, such as transition and rare-earth metals. In such materials the on-site term of the Coulomb interaction is dominant, and other interaction terms can be neglected. The model has been particularly useful in gaining insight to the Mott-transition. Despite sometimes taunted a spherical cow by the experimental physicist because of its qualitative nature, the Hubbard model is complex to the degree that even its equilibrium phase diagram remains an active research topic, and a serious computational challenge at that. An exception to this rule are one dimensional systems, where an analytical equilibrium solution is offered by the Bethe ansatz and the dynamics of the model can be simulated with remarkably efficient numerical methods such as density matrix renormalization group (DMRG) [51] and time evolving block decimation (TEBD) [52].

Let us begin the construction of the Hubbard model from the Bloch theorem which states that the non-interacting single-particle eigenfunctions in a periodic potential V_L can be written in the form

$$\psi_{n\mathbf{k}}(\mathbf{r}) = e^{i\mathbf{k}\cdot\mathbf{r}} u_{n\mathbf{k}}(\mathbf{r}). \tag{2.4}$$

In the expression above, $\mathbf{k}$ is a wave vector, n is the band index and $u_{n\mathbf{k}}$ is a function with the same periodicity as the potential $V_L(\mathbf{r})$. For a given band n, the corresponding eigenenergies $\epsilon_n(\mathbf{k})$ are continuous functions of

k and periodic with respect to any reciprocal lattice vector.

The Wannier functions are a complementary set of (non-interacting) single-particle eigenfunctions which can be defined with the help of the Bloch basis as

$$w_{ni}(\mathbf{r}) = \frac{1}{\sqrt{N_L}} \sum_{\mathbf{k}} e^{-i\mathbf{k}\cdot\mathbf{r}_i} \psi_{n\mathbf{k}}(\mathbf{r}). \tag{2.5}$$

The Wannier function w_{ni} is localized around a single lattice site i, with the localization becoming stronger with increasing lattice depth. Thus, in deep lattices the Wannier functions give the closest possible formal description to the intuitive notion of having "well-defined point-wise particles" in the lattice.

The Hamiltonian of interacting fermions subjected to a lattice potential $V_L(\mathbf{r})$ is

$$\begin{aligned} H = &\sum_{\sigma} \int d\mathbf{r} \Psi_\sigma^\dagger(\mathbf{r}) \left(-\frac{\hbar^2 \nabla_{\mathbf{r}}^2}{2m} + V_L(\mathbf{r}) - \mu_\sigma \right) \Psi_\sigma(\mathbf{r}) \\ &+ g \int d\mathbf{r} \Psi_\uparrow^\dagger(\mathbf{r}) \Psi_\downarrow^\dagger(\mathbf{r}) \Psi_\downarrow(\mathbf{r}) \Psi_\uparrow(\mathbf{r}). \end{aligned} \tag{2.6}$$

Here, the interaction is described by a contact potential characterized by its strength $g = \frac{2\pi\hbar^2 a_s}{m}$, where a_s is the s-wave scattering length and m the mass of the atoms (or twice the reduced mass for mass-imbalanced mixtures) [53]. A basic assumption of the Hubbard model is the reduction of the problem to a single (i.e. lowest) band. This assumption is valid if the band gap between the lowest and the first excited band is large in comparison to the width of the lowest band, the temperature, and the interaction energy scale set by the on-site interaction U which we define more precisely in the following. Under these criteria, we may rewrite the field operators Ψ in the Wannier basis and truncate the representation to the lowest band, i.e. take

$$\Psi_\sigma(\mathbf{r}) = \sum_i w_{0,\mathbf{r}_i}(\mathbf{r}) \hat{c}_{i,\sigma}, \tag{2.7}$$

where $\hat{c}_{i,\sigma}$ now is the annihilation operator corresponding to the Wannier state $w_{0,\mathbf{r}_i}$. As a result, the the Hamiltonian reduces to

$$H = -\sum_{i \neq j,\sigma} J_{ij} \hat{c}_{i\sigma}^\dagger \hat{c}_{j\sigma} - \sum_{i\sigma} \mu_\sigma \hat{c}_{i\sigma}^\dagger \hat{c}_{i\sigma} + \sum_{ijmn} U_{ijmn} \hat{c}_{i\uparrow}^\dagger \hat{c}_{j\downarrow}^\dagger \hat{c}_{m\downarrow} \hat{c}_{n\uparrow}, \tag{2.8}$$

where the hopping J_{ij} and the interaction U_{ijmn} are defined as

$$J_{ij} = -\int d\mathbf{r} w_{0,i}^*(\mathbf{r}) \left(-\frac{\hbar^2 \nabla_{\mathbf{r}}^2}{2m} + V_L(\mathbf{r}) - \mu_\sigma \right) w_{0,j}(\mathbf{r}), \tag{2.9}$$

$$U_{ijmn} = g \int d\mathbf{r} w_{0,i}^*(\mathbf{r}) w_{0,j}^*(\mathbf{r}) w_{0,m}(\mathbf{r}) w_{0,n}(\mathbf{r}). \tag{2.10}$$

In Equation (2.8), the term J_{ii} has been redefined as the chemical potential μ_σ. Assuming that the lattice is sufficiently deep and the Wannier functions sufficiently localized, only the hopping term between nearest neighbouring lattice sites, the chemical potential, and the on-site interaction term are significant, resulting in the Hubbard Hamiltonian

$$H = -\sum_{\langle ij\rangle\sigma} J_{ij}\hat{c}^\dagger_{i\sigma}\hat{c}_{j\sigma} - \sum_{i\sigma}\mu_\sigma c^\dagger_{i\sigma}c_{i\sigma} + U\sum_i c^\dagger_{i\uparrow}c^\dagger_{i\downarrow}c_{i\downarrow}c_{i\uparrow}, \tag{2.11}$$

where $U = U_{iiii}$ and $\langle ij\rangle$ restricts the indices to nearest neighboring lattice sites. In typical experiments on quantum gases, the first discarded kinetic and interaction terms are at least an order of magnitude smaller than U and J above. Here, the fact that the interaction in an atomic gas is described by a contact potential is a significant difference to electrons with Coulomb interaction with regard to truncating the interaction to the local term.

In the context of quantum gases the external trapping potential $V_T(\mathbf{r})$ is typically described by adding to the Hubbard Hamiltonian a site-dependent local potential V_i defined as

$$V_i = \int d\mathbf{r} V_T(\mathbf{r}) w^*_{0,i}(\mathbf{r}) w_{0,i}(\mathbf{r}). \tag{2.12}$$

To a very good approximation $V_i = V_T(\mathbf{r}_i)$.

In general, the computation of the Hubbard model parameters is a numerical task largely dependent on finding the set of maximally localized Wannier functions from the Bloch wave-functions of the lattice. However, for a sufficiently deep optical lattice analytical formulae for J and U can be given. Consider a cubic lattice pontential of the form

$$V_L(\mathbf{r}) = \sum_{i=x,y,z} V_i E_R \sin^2(k_L \hat{\mathbf{e}}_i \cdot \mathbf{r}), \tag{2.13}$$

where $\hat{\mathbf{e}}_i$ with $i \in \{x, y, z\}$ are the Cartesian unit vectors. The hopping parameter can be estimated by mapping the single particle Schrödinger equation to the Matthieu equation, for which asymptotic expressions for the widths of the eigenvalue bands are known. This approach yields the following expression

$$J_i = \frac{4}{\sqrt{\pi}} E_R \left(\frac{V_i}{E_R}\right)^{3/4} \exp\left(-2\sqrt{V_i/E_R}\right). \tag{2.14}$$

Alternatively, the band-width can be computed numerically from the single particle Schrödinger equation. For the on-site interaction U, an analytical estimate can be obtained by approximating the lattice potential of

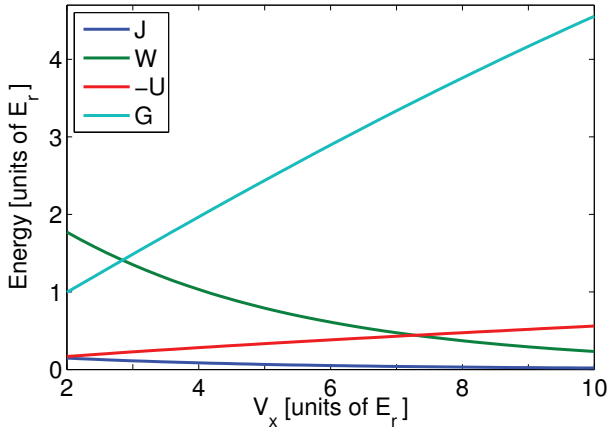

Figure 2.2. The Hubbard model parameters hopping J and interaction strength U as a function of the lattice depth for ^{6}Li in a cubic optical lattice with laser wave length $\lambda_L = 1064$ nm. We also give the band width W and the band gap G. The recoil energy is here $E_r/k_b = 1.4$ μK and the scattering length is fixed at $a_s = -200a_0$ with a_0 the Bohr radius. Above $V_x = 3.0E_R$, the lattice potential is deep in the sense that the higher bands can be neglected and the Hubbard model regarded as a good approximation.

a single site with a harmonic oscillator with the frequency $\omega_i = 2\sqrt{V_i}\frac{E_R}{\hbar}$, resulting in

$$U = \sqrt{\frac{8}{\pi}} k_L a_s (V_x V_y V_z)^{1/4} E_R. \tag{2.15}$$

The approximate formulae above illustrate how the Hubbard model parameters can be tuned experimentally. The hopping is tuned by the lattice potential height V_i. Increasing V_i creates a tighter confinement at each lattice site. Therefore, the individual Wannier functions are narrowed down towards a single lattice site, their overlap is reduced, and as a result the hopping decreases. The on-site interaction U is affected both by the potential height V_i and the s-wave scattering length a_s. The effect of the potential height is again understood from the fact that the Wannier functions are more localized in deeper lattices. Thus, particles at the same lattice site have a stronger overlap, and hence, a stronger interaction. The s-wave scattering length a_s, which characterizes the interaction strength of two atoms in free space appears as a multiplicative factor in the expression of U. The scattering length can be tuned by controlling the Feshbach resonance of the two-body scattering, typically by the external magnetic field strength [4]. In Figure 2.2 we plot the Hubbard model parameters for a cubic lattice containing a two-component gas of ^6Li.

In the discussion above, the hopping parameter J and the local potential

V_i are given as spin-independent, but in general it is possible that these quantities depend on the spin state σ. There are essentially two different possible sources for such state-dependence. Firstly, if the spin states have different optical properties then according to Equation 2.1 the same laser field induces a different potential for these states. If the relevant optical transitions are well-separated, a technically more involved arrangement of a separate laser for each state is also a possibility. Moreover, if the system is constructed of two different elements or isotopes, then the mass difference of the components also affects the parametrization of the Hubbard model. The possibility of the spin-dependent Hubbard model is relevant to realizing the spin-asymmetric Josephson effect in optical lattices as discussed in Publication IV. Finally, let us note that the spin-dependence of the hopping is not a necessary consequence of the mass imbalance alone, as this difference can be canceled by the state-dependent optical potential with a specific laser frequency.

3. Superfluidity

Superfluidity refers to a state of matter in which a fluid has zero viscosity. It is a truly fascinating macroscopic consequence of quantum many body physics. Superconductivity, which is defined as the zero electrical resistance of a solid, is very closely related to superfluidity, and can essentially be regarded as the superfluidity of charged particles. In fact, there is a deeper connection between these two phenomena, as it is well-established that certain forms of superconductivity and superfluidity are caused by the same microscopic mechanism. [54]

All forms of superfluidity owe their origins to quantum mechanical and quantum statistical effects, and here, the discussion may essentially be divided to two cases according to the quantum statistics of the particles making up the superfluid. Thus, we have bosonic and fermionic superfluidity.

For roughly half a century, liquid ^{4}He was the only known bosonic superfluid [54], but during the past twenty years, the phenomenon has also been observed in ultracold Bose gases [1, 2, 3, 13] and exciton-polariton condensates [55]. Superfluidity of bosons is related to Bose-Einstein condensation (BEC), the macroscopic occuption of a single particle eigenstate – typically this eigenstate is the lowest one in energy, and unique. Very simplistically, the condensate then corresponds to a single macroscopic wave-function whose dynamics all the particles in the system follow without dissipation, giving rise to superfluidity. Under closer scrutiny, the connection of Bose-Einstein condensation to superfluidity turns out to be rather more delicate. To illustrate this, define the condensate fraction as the number of particles in the macroscopically occupied state relative to the total particle number, and similarly, define the superfluid fraction as the relative number of particles participating in a dissipationless flow. Now, in a weakly interacting Bose gas these two quantities are equal, as

has been demonstrated e.g. in a BEC of ^{87}Rb. However, in superfluid ^{4}He the condensate fraction is only about $10\ \%$ though the entire system is superfluid, and on the other hand, a BEC of a non-interacting Bose gas would not demonstrate superfluidity at all.

In fermionic systems, the Pauli exclusion principle prevents the multiple occupation of any single particle eigenstate, and thus, a BEC of single particles is strictly forbidden. Yet, there are several known examples of fermionic superfluidity. Superconductivity of electrons, arguably the most useful form of superfluidity, is the most obvious example. Superfluidity has also been observed in liquid ^{3}He [54] and ultracold Fermi gases [1, 2, 3, 13], and there is also a substantial amount of evidence for superfluidity in nuclear matter and neutron stars [56].

The key concept in understanding fermionic superfluidity is that of Cooper pairing which refers to the formation of a specific type of bound state between two fermions. In Cooper pairing, the presence of the Fermi sea contributes significantly to the bound state formation by making some of the possible scattering states inaccessible because of Pauli exclusion. The simplest way to explain the superfluidity of Cooper paired fermions would then be to regard Cooper pairs as elementary bosons forming a BEC which in turn leads to superfluidity. However, we find that this analogy needs to be taken with a grain of salt, if we examine the distinction between Cooper pairs and elementary bosons in the spirit of section 1.1. The Cooper pair radius in superconducting metals is known to be typically on the order of $r_0 = 1\ \mu\mathrm{m}$, whereas their density, i.e. half the condensate fraction times electron density, is on the order of $n = 0.5 \times 10^{-3\ldots-4} \times 10^{23}\ \frac{1}{\mathrm{cm}^3}$, in which case we have $nr_0^3 = 0.5 \times 10^7$ and the Cooper pairs overlap significantly. Thus, Cooper pairs in metals may not in general be regarded as elementary bosons. This picture coincides well with the fact that the pair is held together by the Pauli blocking of scattering states by other fermions in the system. Thus, the notion of Cooper pairing needs to be generalized very carefully from the two-body problem to the many-body problem, and this generalization is achieved by the celebrated Bardeen-Cooper-Schrieffer (BCS) theory [57].

3.1 Spin-polarized fermionic superfluidity

Superconductivity and magnetization are usually thought to be natural enemies. The superconductivity of metals originates from BCS pairing

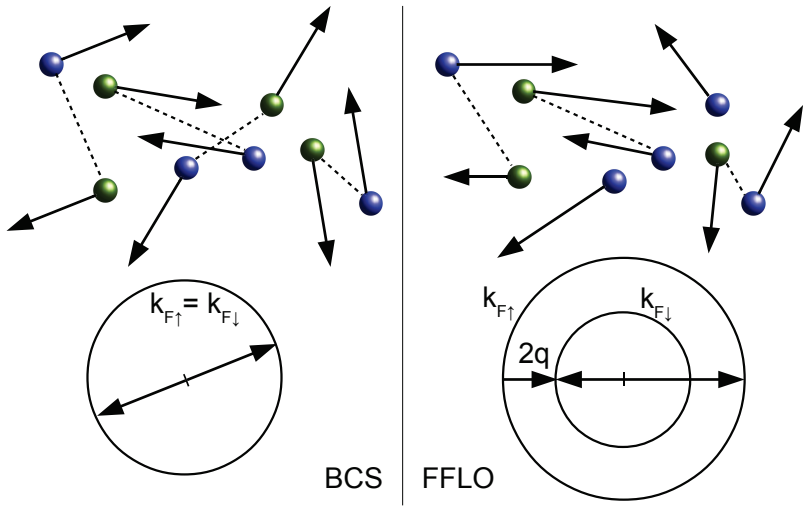

Figure 3.1. In the BCS state Cooper pairing occurs between fermions of opposite spin and momentum, predominantly in the vicinity of the Fermi surface. The introduction of spin-polarization creates a difference between the Fermi momenta of the spin components, $k_{F\uparrow} > k_{F\downarrow}$, which is detrimental to the pairing at opposite momenta. In the FFLO mechanism, a finite pairing momentum is introduced to connect the Fermi surfaces better. The finite center of mass momentum of the Cooper pairs is visible in the spatial modulation of the order parameter.

of the s-wave singlet type, i.e. a Cooper pair in a metal is formed by two electrons with opposite spins. On the other hand, the magnetization of a metal would predominantly require an excess of electrons in one of the spin-eigenstates, a spin-polarization, which of course should not occur in a system consisting of spin-singlet pairs [58, 59].

The implications of the coexistence of superconductivity and magnetization were first considered by Fulde and Ferrell [60], and Larkin and Ovchinnikov [61, 62]. The main idea of both works was that giving Cooper pairs a finite center of mass momentum alleviates the Fermi surface mismatch between spin-up and spin-down electrons caused by magnetization, making the coexistence of magnetization and superfluidity possible. This principle which results in the Fulde-Ferrell-Larkin-Ovchinnikov (FFLO) state is illustrated in Figure 3.1.

The finite center of mass momentum leads to a spatially non-uniform order parameter. Originally, Fulde and Ferrell studied an order parameter of the plane wave form, $\Delta(\mathbf{r}) = \Delta_0 e^{2i\mathbf{q}\cdot\mathbf{r}}$, which involves exactly one possible momentum for the pairing. Larkin and Ovchinnikov, on the other hand, studied a broader set of order parameters and concluded that an order parameter of the cosine form, $\Delta(\mathbf{r}) = \Delta_0 \cos(2\mathbf{q}\cdot\mathbf{r})$, would quite gen-

erally be the optimal one. Now, the detailed form of the order parameter leads to some important physical differences. In the Fulde-Ferrell (FF) scenario, the condensate would carry a finite current as a direct result of all Cooper pairs having the same momentum. On the other hand, the Bloch theorem stipulates that the equilibrium state of the system cannot carry any current. In the FF scenario, the excess spin-population is also carrying a finite momentum directed on average opposite to the condensate momentum. At equilibrium there is a balance between these two currents. On the other hand, the Larkin-Ovchinnikov (LO) order parameter $\Delta(\mathbf{r}) = \Delta_0 \cos(2\mathbf{q} \cdot \mathbf{r})$ corresponds to two pairing momenta in opposite directions and on this merit alone, there is no net current in the system. However, there is another interesting feature associated with this order parameter. Namely, corrections to the density are proportional to the absolute value squared of the order parameter, and thus, in such a state the density would obtain a periodic modulation with half the wavelength of the order parameter.

As already stated, in general an order parameter of the cosine form is the energetically more favorable than the plane wave. However, the plane wave ansatz does represent some of the qualitative properties of a polarized superfluid fairly well, and can be dealt with in an analytically closed form. Therefore the plane wave ansatz is a reasonable choice for many theoretical considerations. In this context, it is interesting to note that in recent theoretical works it has been suggested that the presence of spin-orbit coupling could tip the scale in favor of the plane wave order parameter [63, 64].

So far, the experimental evidence for the existence of the FFLO state has been inconclusive. The main reason is that in metallic superconductors the FFLO state would emerge as a function of the external magnetic field only very close to the Pauli paramagnetic limit (also known as the Chandrasekhar-Clogston limit), i.e. the magnetic field strength where the Zeeman splitting of the spin-states is sufficiently large for pair breaking. However, in the vast majority of superconducting materials the transition to normal state in an external magnetic field is caused by orbital effects far below the paramagnetic limit. Moreover, any candidate system should be extremely clean as the FFLO state is very sensitive to impurities.[1]

[1] An additional hurdle in finding the FFLO state is that the majority of superconducting materials are type-II superconductors, in which the transition to normal state is preceded by a transition to the Abrikosov vortex lattice state where a finite magnetic flux passes through the superconductor through vortex cores.

Based on these arguments, the search for the FFLO state has been most active in heavy fermion systems, where the paramagnetic limit is more relevant because of the large effective mass of the electrons, and in systems where orbital effects are suppressed due to reduced dimensionality such as organic superconductors. The most promising results have been reported for the heavy fermion compound $CeCoIn_5$ [65, 66, 67, 68] and certain organic fulvalene-superconductors [69, 70].

The criteria above show up in a very different light in the context of quantum gases. In a quantum gas, the occupation number of each pseudo spin component can be fixed independently, which corresponds to fixing the chemical potential of each component. Thus, the chemical potential difference is the analogy of the Zeeman splitting of electrons, with the exception that there are no orbital effects caused by the external magnetic field in the system. Moreover, the quantum gas setups are extremely clean. This suggests that quantum gases offer a very promising testbed for the FFLO scenario, and while the state itself has not yet been realized important milestones with population imbalanced systems have been achieved [14, 15, 71]. Moreover, strong arguments have been presented to indicate that in deep optical lattices the nesting of Fermi surfaces would make the FFLO state significantly more stable, and realizable in a much broader parameter region than in continuum [72, 73].

In the following, we present the mean-field formalism for the Fulde-Ferrell ansatz with the plane wave order parameter $\Delta(\mathbf{r}) = \Delta_0 e^{2i\mathbf{q}\cdot\mathbf{r}}$. This discussion provides the starting point for Publication II. Here, we assume that the system is described by the Hubbard model (2.11) on a cubic lattice with N_L lattice sites and a periodic boundary condition.

The single particle Green's function is defined in the finite temperature Matsubara Green's function formalism as follows [74, 75, 76]

$$G(1,1') = -\left\langle T_\tau \left(\hat{c}(1)\hat{c}^\dagger(1') \right) \right\rangle . \tag{3.1}$$

Here, use the notation 1 for the variables $\mathbf{r}_1\tau_1\sigma_1$, while T_τ is the time ordering operator and the brackets denote the thermodynamic average defined for the operator $\hat{O}$ as

$$\left\langle \hat{O} \right\rangle = \frac{\mathrm{Tr}\left\{ e^{-\beta H}\hat{O} \right\}}{\mathrm{Tr}\left\{ e^{-\beta H} \right\}}, \tag{3.2}$$

where $\beta = \frac{1}{k_b T}$ is the inverse temperature with k_b the Boltzmann constant and T the temperature. We describe the system in Nambu formalism with an extended spin index $\sigma \in \{1,2,3,4\}$ by setting $\hat{c}_3 = \hat{c}_1^\dagger$ and $\hat{c}_4 = \hat{c}_2^\dagger$.

Thus, the anomalous Green's functions with two creation or two annihilation operators are also defined by Equation (3.1). These are essential for describing pairing correlations on the mean field level.

The single particle Green's function has the following equation of motion

$$\int G_0^{-1}(1,\bar{1})G(\bar{1},1') = \delta(1,1') + \int \Sigma(1,\bar{1})G(\bar{1},1'). \tag{3.3}$$

The integral sign is a shorthand notation for summation over position and spin as well as integration over time, while variables of summation and integration are indicated by the overbar. The inverse non-interacting single particle Green's function is

$$G_0^{-1}(1,1') = \left(-\frac{\partial}{\partial\tau} + \mu(1)\right)\delta(1,1') + J_{\sigma,\mathbf{r}\mathbf{r}'}\delta(\tau_1-\tau_1')\delta_{\sigma\sigma'}, \tag{3.4}$$

where the hopping J_σ is in matrix form over position, and for the extended spin index we have $\mu_3 = -\mu_1 + U_{12}$, $\mu_4 = -\mu_2 + U_{12}$, $J_3 = -J_1$ and $J_4 = -J_2$. Furthermore, $\delta(1,1')$ stands for the Dirac and Kronecker delta for continuous and discrete variables, respectively. For a general two-body interaction the self-energy Σ is defined as

$$\Sigma(1,1') = -\int V(1,\bar{1})G_2(1,\bar{1}^-,\bar{2},\bar{1}^+)G^{-1}(\bar{2},1'). \tag{3.5}$$

Here the notations τ^+ and τ^- specify the time-ordering $\tau^+ > \tau > \tau^-$ and imply taking the limit $\tau^\pm \to \tau$, while the two particle Green's function G_2 is defined as

$$G_2(1,2,3,4) = -\left\langle T_\tau\left(\hat{c}(1)\hat{c}(2)\hat{c}^\dagger(4)\hat{c}^\dagger(3)\right)\right\rangle. \tag{3.6}$$

In the Hubbard model the interaction is local both in time and space, i.e. $V(1,2) = U_{\sigma_1\sigma_2}\delta(\mathbf{r}_1,\mathbf{r}_2)\delta(\tau_1-\tau_2)$, with $U_{34} = U_{12} = U$ for the extended index.

In the Hartree-Fock-Gor'kov mean-field approximation the self energy is

$$\Sigma = -U\delta(\mathbf{r}_1\tau_1,\mathbf{r}_1'\tau_1')\begin{bmatrix} -G_{22} & G_{12} & 0 & -G_{14} \\ G_{21} & -G_{11} & -G_{23} & 0 \\ 0 & -G_{32} & -G_{44} & G_{34} \\ -G_{41} & 0 & G_{43} & -G_{33} \end{bmatrix}. \tag{3.7}$$

Here, the Green's functions appearing in Σ have the variables $(\mathbf{r}_1\tau_1, \mathbf{r}_1\tau_1^+)$.

We may include the Hartree terms on the diagonal of the self-energy matrix to the chemical potentials if the density of the system is uniform. The Fock-exchange terms G_{12}, G_{21}, G_{34} and G_{43} can be neglected in the case

of the Fermi gas, since spin-flipping is energetically highly unfavorable at experimentally relevant magnetic field strengths. Finally we introduce the key element of the mean field FFLO theory. We assume that the pairing fields of the self-energy have an oscillating structure

$$\Sigma = \delta(\mathbf{r}_1\tau_1, \mathbf{r}_1'\tau_1')\Delta \begin{bmatrix} 0 & 0 & 0 & e^{2i\mathbf{q}\cdot\mathbf{r}_1} \\ 0 & 0 & -e^{2i\mathbf{q}\cdot\mathbf{r}_1} & 0 \\ 0 & -e^{-2i\mathbf{q}\cdot\mathbf{r}_1} & 0 & 0 \\ e^{-2i\mathbf{q}\cdot\mathbf{r}_1} & 0 & 0 & 0 \end{bmatrix}. \tag{3.8}$$

Here, the FFLO pairing vector is denoted by $\mathbf{q}$. In the special case of $\mathbf{q} = 0$ and $N_1 = N_2$ the system is reduced to the standard BCS description. The case with $\mathbf{q} = 0$ and $N_1 \neq N_2$ is referred to as the breached pair (BP) state [77, 78].

The quantity $\Delta e^{-2i\mathbf{q}\cdot\mathbf{r}_1}$ is the order parameter of the FFLO state. Its magnitude Δ is related to the energy gap of pair breaking excitations. The definition of the self-energy can also be interpreted as the self-consistency condition of the mean field solution. Because of the symmetries of the self-energy, this condition can be expressed with a single equation

$$G_{32}(1, 1^+) = -\frac{1}{U}\Delta e^{-2i\mathbf{q}\cdot\mathbf{r}_1}, \tag{3.9}$$

from which the FFLO gap equation can be derived. The particle number of each spin component, i.e. the number equation, is given by

$$N_\sigma = \sum G_{\sigma\sigma}(\bar{\mathbf{r}}\tau, \bar{\mathbf{r}}\tau^+), \tag{3.10}$$

while the filling fraction is defined as $n_\sigma = N_\sigma/N_L$.

We now proceed to derive a closed algebraic form for the FFLO Green's function in momentum and frequency space. Here, in order to find an algebraically closed set of Fourier components we have to pay particular attention to the broken spatial translation invariance of the self-energy. We define the Fourier transform of the Green's function as

$$\begin{aligned} G(\mathbf{p}_1, \mathbf{p}_2, \omega) = \sum_{\mathbf{r}_1,\mathbf{r}_2} \int_0^\beta d\,(\tau_1 - \tau_2)\, e^{i\omega(\tau_1-\tau_2)} \\ \mathcal{F}(\mathbf{p}_1\cdot\mathbf{r}_1) G(\mathbf{r}_1, \mathbf{r}_2, \tau_1 - \tau_2) \mathcal{F}^\dagger(\mathbf{p}_2\cdot\mathbf{r}_2), \end{aligned} \tag{3.11}$$

where the Fourier transfrom matrix $\mathcal{F}$ is given by

$$\mathcal{F}(\mathbf{p}_1\cdot\mathbf{r}_1) = \begin{bmatrix} e^{-i\mathbf{p}_1\cdot\mathbf{r}_1} & 0 & 0 & 0 \\ 0 & e^{-i\mathbf{p}_1\cdot\mathbf{r}_1} & 0 & 0 \\ 0 & 0 & e^{i\mathbf{p}_1\cdot\mathbf{r}_1} & 0 \\ 0 & 0 & 0 & e^{i\mathbf{p}_1\cdot\mathbf{r}_1} \end{bmatrix}. \tag{3.12}$$

Here, $\mathbf{p}_1$ and $\mathbf{p}_2$ are momenta and ω is the Matsubara frequency $\omega = \frac{(2n+1)\pi}{\beta}$ where n is an integer. The inverse Fourier transformation is

$$G(\mathbf{r}_1, \mathbf{r}_2, \tau_1 - \tau_2) = \frac{1}{\beta N_L} \sum_{\mathbf{p}_1, \mathbf{p}_2, \omega} e^{-i\omega(\tau_1 - \tau_2)} \mathcal{F}^\dagger(\mathbf{p}_1 \cdot \mathbf{r}_1) G(\mathbf{p}_1, \mathbf{p}_2, \omega) \mathcal{F}(\mathbf{p}_2 \cdot \mathbf{r}_2). \tag{3.13}$$

Taking Fourier transform the equation of motion (3.3) for G in the FFLO state we find in the $\sigma_1, \sigma_2 \in \{1, 4\}$ spin-block

$$\begin{bmatrix} i\omega - \xi_1(\mathbf{p}_1) & 0 \\ 0 & i\omega + \xi_2(\mathbf{p}_1) \end{bmatrix} G(\mathbf{p}_1, \mathbf{p}_2, \omega) = \delta_{\mathbf{p}_1, \mathbf{p}_2} I + \Delta \begin{bmatrix} 0 & 1 \\ 1 & 0 \end{bmatrix} G(2\mathbf{q} - \mathbf{p}_1, \mathbf{p}_2, \omega). \tag{3.14}$$

Here $\xi_\sigma(\mathbf{p}) = \epsilon(\mathbf{p}) - \mu_\sigma$ is the single particle dispertion $\epsilon(\mathbf{p})$ relative to the chemical potential. After a relabeling of the momenta, the equation above is inverted as

$$\begin{bmatrix} G_{11}(\mathbf{p}_1, \mathbf{p}_2, \omega) & G_{14}(\mathbf{p}_1, 2\mathbf{q} - \mathbf{p}_2, \omega) \\ G_{41}(2\mathbf{q} - \mathbf{p}_1, \mathbf{p}_2, \omega) & G_{44}(2\mathbf{q} - \mathbf{p}_1, 2\mathbf{q} - \mathbf{p}_2, \omega) \end{bmatrix} = \frac{\delta_{\mathbf{p}_1, \mathbf{p}_2}}{(i\omega - \xi_1(\mathbf{p}_1))(i\omega + \xi_2(2\mathbf{q} - \mathbf{p}_1)) - \Delta^2} \times \begin{bmatrix} i\omega + \xi_2(2\mathbf{q} - \mathbf{p}_1) & \Delta \\ \Delta & i\omega - \xi_1(\mathbf{p}_1) \end{bmatrix}. \tag{3.15}$$

After this, we define the quasiparticle energies $E_\pm$ [60] as

$$E_\pm(\mathbf{p}) = \pm \frac{\xi_1(\mathbf{p}) - \xi_2(2\mathbf{q} - \mathbf{p})}{2} + \sqrt{\left(\frac{\xi_1(\mathbf{p}) + \xi_2(2\mathbf{q} - \mathbf{p})}{2} \right)^2 + \Delta^2}, \tag{3.16}$$

and the coherence factors u and v as

$$u(\mathbf{p}) = \sqrt{\frac{E_+(\mathbf{p}) + \xi_2(2\mathbf{q} - \mathbf{p})}{E_+(\mathbf{p}) + E_-(\mathbf{p})}}, \tag{3.17}$$

$$v(\mathbf{p}) = \sqrt{\frac{E_-(\mathbf{p}) - \xi_2(2\mathbf{q} - \mathbf{p})}{E_+(\mathbf{p}) + E_-(\mathbf{p})}}. \tag{3.18}$$

The FFLO quasiparticle dispersions are plotted in Figure 3.2.

Now, using the notations above we may rewrite Equation (3.15) as

$$\begin{bmatrix} G_{11}(\mathbf{p}_1, \mathbf{p}_2, \omega) & G_{14}(\mathbf{p}_1, 2\mathbf{q} - \mathbf{p}_2, \omega) \\ G_{41}(2\mathbf{q} - \mathbf{p}_1, \mathbf{p}_2, \omega) & G_{44}(2\mathbf{q} - \mathbf{p}_1, 2\mathbf{q} - \mathbf{p}_2, \omega) \end{bmatrix} = \frac{\delta_{\mathbf{p}_1, \mathbf{p}_2}}{i\omega - E_+(\mathbf{p}_1)} \begin{bmatrix} u(\mathbf{p}_1)^2 & u(\mathbf{p}_1)v(\mathbf{p}_1) \\ u(\mathbf{p}_1)v(\mathbf{p}_1) & v(\mathbf{p}_1)^2 \end{bmatrix} + \frac{\delta_{\mathbf{p}_1, \mathbf{p}_2}}{i\omega + E_-(\mathbf{p}_1)} \begin{bmatrix} v(\mathbf{p}_1)^2 & -u(\mathbf{p}_1)v(\mathbf{p}_1) \\ -u(\mathbf{p}_1)v(\mathbf{p}_1) & u(\mathbf{p}_1)^2 \end{bmatrix}. \tag{3.19}$$

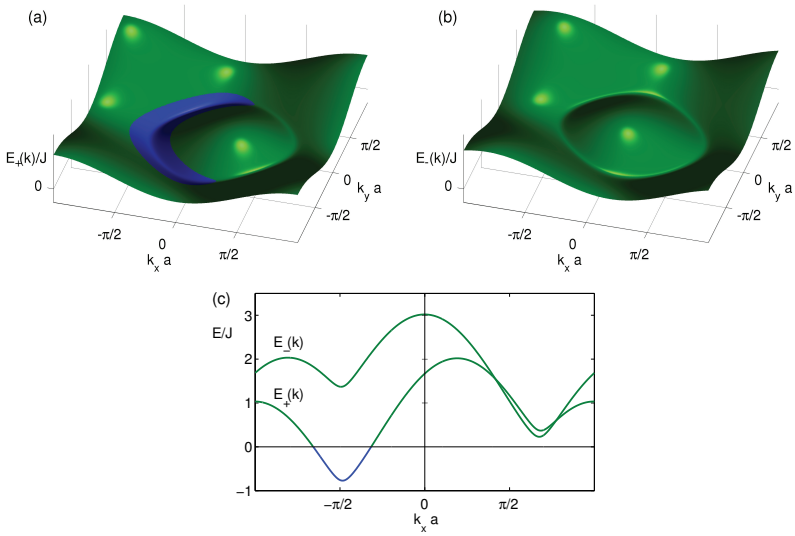

Figure 3.2. The FFLO quasi-particle dispersions (a) $E_+(\mathbf{k})$ and (b) $E_-(\mathbf{k})$ for the plane wave ansatz as given by Equation (3.16) in the $k_z = 0$ plane. Panel (c) gives both the dispersions $E_+(\mathbf{k})$ and $E_-(\mathbf{k})$ for $k_y = k_z = 0$. The negative energies are plotted in blue color and positive in green. The states with $E_+(\mathbf{k}) < 0$ are occupied even at zero temperature, and carry the excess particle number of the majority component. The current carried by these quasi-particles is balanced by the current carried by the condensate so that the total current in the system is zero.

In the spin-block $\sigma_1, \sigma_2 \in \{2, 3\}$, a similar calculation yields the expression

$$\begin{aligned}
&\begin{bmatrix} G_{22}(2\mathbf{q}-\mathbf{p}_1, 2\mathbf{q}-\mathbf{p}_2, \omega) & G_{23}(2\mathbf{q}-\mathbf{p}_1, \mathbf{p}_2, \omega) \\ G_{32}(\mathbf{p}_1, 2\mathbf{q}-\mathbf{p}_2, \omega) & G_{33}(\mathbf{p}_1, \mathbf{p}_2, \omega) \end{bmatrix} \\
=&\frac{\delta_{\mathbf{p}_1,\mathbf{p}_2}}{i\omega - E_-(\mathbf{p}_1)} \begin{bmatrix} u(\mathbf{p}_1)^2 & -u(\mathbf{p}_1)v(\mathbf{p}_1) \\ -u(\mathbf{p}_1)v(\mathbf{p}_1) & v(\mathbf{p}_1)^2 \end{bmatrix} \\
+&\frac{\delta_{\mathbf{p}_1,\mathbf{p}_2}}{i\omega + E_+(\mathbf{p}_1)} \begin{bmatrix} v(\mathbf{p}_1)^2 & u(\mathbf{p}_1)v(\mathbf{p}_1) \\ u(\mathbf{p}_1)v(\mathbf{p}_1) & u(\mathbf{p}_1)^2 \end{bmatrix}.
\end{aligned} \tag{3.20}$$

Thus, the normal Green's functions are diagonal in momentum space, and one could revert back to the more simple notation of $G_{\sigma\sigma}(\mathbf{p}_1, \omega) = G_{\sigma\sigma}(\mathbf{p}_1, \mathbf{p}_2, \omega)$ for $\mathbf{p}_1 = \mathbf{p}_2$. However, the anomalous functions are non-diagonal because of the oscillatory structure of the pairing field, and one has to carry the FFLO pairing momentum in the equations involving Green's functions of this type. Notice that the remaining eight Green's functions $G_{\sigma\nu}$ vanish in the adopted approximation.

Using the results above, we may write down the gap Equation (3.9) and the number Equations (3.10) in a self-contained form. The inverse Fourier transform of $G_{32}(1, 1^+)$ is

$$G_{32}(\mathbf{r}\tau, \mathbf{r}\tau^+) = \frac{1}{N_L} \sum_{\mathbf{p}} e^{-2i\mathbf{q}\cdot\mathbf{r}} u(\mathbf{p})v(\mathbf{p})[1 - n_F(E_+(\mathbf{p})) - n_F(E_-(\mathbf{p}))], \tag{3.21}$$

in which the Fermi distribution n_F has been obtained from the Matsubara summation

$$n_F(E) = \frac{1}{\beta} \sum_{\omega} \frac{e^{i\omega(\tau^+ - \tau)}}{i\omega - E}. \tag{3.22}$$

Therefore, we may write the gap Equation as

$$-\frac{\Delta}{U} = \frac{1}{N_L} \sum_{\mathbf{p}} u(\mathbf{p})v(\mathbf{p})[1 - n_F(E_+(\mathbf{p})) - n_F(E_-(\mathbf{p}))]. \tag{3.23}$$

Similarly, we obtain the number Equations

$$n_1 = G_{11}(\mathbf{r}\tau, \mathbf{r}\tau^+) = \frac{1}{N_L} \sum_{\mathbf{p}} u(\mathbf{p})^2 n_F(E_+(\mathbf{p})) + v(\mathbf{p})^2[1 - n_F(E_-(\mathbf{p}))], \tag{3.24}$$

and

$$n_2 = G_{22}(\mathbf{r}\tau, \mathbf{r}\tau^+) = \frac{1}{N_L} \sum_{\mathbf{p}} u(\mathbf{p})^2 n_F(E_-(\mathbf{p})) + v(\mathbf{p})^2[1 - n_F(E_+(\mathbf{p}))]. \tag{3.25}$$

Finally, we give an expression for the expected value of the current. Using this expression, it is possible to fix the value of the FFLO vector $\mathbf{q}$ from the condition that the total current must vanish at equilibrium.[2] The expected value of the current along each axis is [74]

$$\mathbf{j}_i = iJ \sum_{\mathbf{r},\sigma} \sum_{\lambda=\pm 1} \lambda G_\sigma(\mathbf{r}, \mathbf{r} + \lambda a \hat{\mathbf{e}}_i, 0^-), \tag{3.26}$$

where a is the lattice constant and $\hat{\mathbf{e}}_i$ a unit vector along the i-axis with $i \in \{x, y, z\}$. This equation can be written in terms of the quasiparticle energies and coherence factors as

$$\begin{aligned}\mathbf{j}_i = 2J \sum_{\mathbf{p}} \sin(\mathbf{p} \cdot a\hat{\mathbf{e}}_i) \big\{ & u(\mathbf{p})^2 [n_F(E_+(\mathbf{p})) + n_F(E_-(\mathbf{p}))] \\ & + v(\mathbf{p})^2 [2 - n_F(E_+(\mathbf{p})) - n_F(E_-(\mathbf{p}))] \big\}. \end{aligned} \tag{3.27}$$

The results above are utilized to describe the FFLO ground state in the linear response calculations of Publication II. From the point of view of numerics, the accurate implementation of the gap equation (3.23) consistently with the numerical implementation of the linear response formulae is of particular importance – even small inconsistencies may lead to the qualitatively wrong result of a gapped collective mode dispersion. This detail is connected to the self-consistency of the linear response theory as discussed in Chapter 4, and in particular, to section 4.2.1 where we show analytically that the collective mode spectrum is always gapless. The concepts related to spin-polarized superfluidity discussed in this chapter are also central to Publication III and Publication V. In these works we utilize numerically heavier methods to go beyond the static mean-field approach. The FFLO state found in these works is much more similar to the LO state with an approximately sinusoidal order parameter and oscillating density profile than to the FF state examined above. The mean-field treatment of fermionic superfluidity above contains the BCS theory as a limiting case, and this of course offers the starting point for the studies of the Josephson effect presented in Publication I and Publication IV.

[2] However, in computing the phase diagram of the system, an alternate approach based on minimizing the free energy of the system is preferable.

4. Linear response theory

Perturbation theory is a very general approach to describe physical systems that cannot be solved with exact analytical methods. The main idea is to divide the problem at hand into a more easily described system and a perturbation acting on this simpler system, and then, to estimate how this perturbation changes the solution. In linear response theory it is assumed that the change in the system is directly proportional to the strength of the perturbation. This approach is particularly useful if the unperturbed system is independent of time, and moreover, can be considered to be in thermodynamic equilibrium. In such cases determining the non-equilibrium properties of the perturbed system can be reduced to equilibrium quantities which typically are substantially easier to compute. However, it is worth emphasizing that in spite of the apparent simplicity of the unperturbed equilibrium system, its solution may still be known only up to an approximation. This in turn implies that the the perturbation theory has to be constructed consistently with respect to the approximations taken for the equilibrium system. In the following, we outline the linear response formalism with a particular focus on the self-consistency of the theory as defined by Kadanoff and Baym [79, 80].

For a quantum many-body system initially in thermodynamic equilibrium, the linear change in the expected value of an observable $\hat{O}$ in response to a perturbation represented by the operator $H'(t)$ follows the Kubo formula [74, 75, 76]

$$\delta \left\langle \hat{O}(t) \right\rangle = -i \int_{-\infty}^{\infty} dt' \, \Theta(t - t') \left\langle \left[\hat{O}(t), H'(t') \right] \right\rangle . \tag{4.1}$$

Here, the perturbation $H'(t)$ is assumed zero for $t < 0$, and $\Theta(t)$ is the Heaviside step function. The time evolution of the operators inside the commutator is given in the interaction picture. In the following, both H'

and $\hat{O}$ are single-particle operators of the generic form

$$H' = \int \phi(\bar{1},\bar{2})\psi^\dagger(\bar{1})\psi(\bar{2}), \tag{4.2}$$

$$\hat{O} = \int \tilde{\phi}(\bar{1},\bar{2})\psi^\dagger(\bar{1})\psi(\bar{2}). \tag{4.3}$$

For instance in the FFLO density response study of Publication II, the perturbing field is diagonal in position and spin, i.e. couples locally to the density of the system, and there are two observables of interest, the densities of each spin component in the system:

$$\begin{aligned} H' &= \int \left(\phi_1(\bar{\mathbf{r}},t)\psi_1^\dagger(\bar{\mathbf{r}},t)\psi_1(\bar{\mathbf{r}},t) + \phi_2(\bar{\mathbf{r}},t)\psi_2^\dagger(\bar{\mathbf{r}},t)\psi_2(\bar{\mathbf{r}},t)\right), \\ \hat{O}_1 &= \psi_1^\dagger(\mathbf{r},t)\psi_1(\mathbf{r},t), \\ \hat{O}_2 &= \psi_2^\dagger(\mathbf{r},t)\psi_2(\mathbf{r},t). \end{aligned} \tag{4.4}$$

In the case of single particle operators the integrand of the Kubo formula is a retarded two-body correlation function, or linear response function, multiplied by the strength of the perturbing field. The retarded linear response function is defined as

$$L_{\sigma_1\sigma_2\sigma_3\sigma_4}(\mathbf{r},\mathbf{r}',t-t') = -i\theta(t-t')\left\langle\left[\psi_{\sigma_3}^\dagger(\mathbf{r},t)\psi_{\sigma_1}(\mathbf{r},t), \psi_{\sigma_4}^\dagger(\mathbf{r}',t')\psi_{\sigma_2}(\mathbf{r}',t')\right]\right\rangle. \tag{4.5}$$

The standard strategy for computing the linear response function is to first solve the corresponding time-ordered Matsubara correlation function. From this function, the real-time retarded correlation function can be obtained by means of analytical continuation. From here on we continue using the Matsubara formalism.

In Publication I and Publication II we employ the Kadanoff-Baym formalism [79, 80] to derive the linear response function. This formalism provides a rigorous framework for deriving conserving and thermodynamically consistent approximations for the many-body problem. Here, a conserving approximation is such that it obeys the conservation laws arising from the symmetries of the physical system while thermodynamical consistency means that the partition function is unique, or in other words, that the direct evaluation of observables and their calculation by differentiating the partition function yield the same result. These important properties are not necessarily true for any approximation. In fact, the construction of such a theory is possible if and only if the self-energy of the system is Φ-derivable. This means that there exists a closed functional of the Green's function $\Phi(G)$ from which the self-energy can be obtained as

a variational derivative as follows

$$\Sigma(1,1') = \frac{\delta\Phi(G)}{\delta G(1',1)}. \tag{4.6}$$

This definition of Φ-derivability is equivalent with the following vanishing curl condition for the self-energy

$$\frac{\delta\Sigma(1,1')}{\delta G(2',2)} = \frac{\delta\Sigma(2,2')}{\delta G(1',1)}. \tag{4.7}$$

From this condition, one can directly inspect that for instance the Hartree-Fock-Bogoliubov mean-field approximation introduced in Section 3.1 is indeed Φ-derivable. Thus, conserving Linear response theories can be constructed for this approximation.

For all Φ-derivable theories, the linear response function can be expressed as the variational derivative of the Green's function with respect to the external field ϕ evaluated at $\phi = 0$

$$L(12,1'2') = \left(\frac{\delta G(1,1')}{\delta\phi(2',2)}\right)_{\phi=0}. \tag{4.8}$$

For example the density is given by $n_{\sigma_1}(\mathbf{r}_1\tau_1) = G(1,1^+)$ so $L(12,1^+2^+)$ would give the density response function. Rather than solving the non-equilibrium $G(U)$ to solve this derivative, one can utilize the Dyson equation

$$G^{-1}(1,1') = G_0^{-1}(1,1') - \phi(1,1') - \Sigma(1,1') \tag{4.9}$$

to obtain the variational derivative of the inverse propagator. Now, by taking the variational derivative of the identity $\int G(1,\bar{1})G(\bar{1},1')^{-1} = \delta(1,1')$ one obtains the linear response function as

$$L(12,1'2') = \int\left(G(1,\bar{3})\left(\frac{\delta\phi(\bar{3},\bar{4})}{\delta\phi(2',2)} + \frac{\delta\Sigma(\bar{3},\bar{4})}{\delta\phi(2',2)}\right)G(\bar{4},1')\right)_{\phi=0}. \tag{4.10}$$

This equation is still an implicit equation for the linear response function as the self-energy is expressed in terms of the Green's function and thus derivatives of the Green's function appear on the right hand side as well. Indeed, using the chain rule of differentiantion this equation is rewritten as

$$\begin{aligned} L(12,1'2') = &\int G(1,\bar{3})_{\phi=0}G(\bar{4},1')_{\phi=0}\left(\frac{\delta\phi(\bar{3},\bar{4})}{\delta\phi(2',2)}\right)_{\phi=0} \\ &+ \int G(1,\bar{3})_{\phi=0}G(\bar{4},1')_{\phi=0}\left(\frac{\delta\Sigma(\bar{3},\bar{4})}{\delta G(\bar{5},\bar{6})}\right)_{\phi=0} L(\bar{5}2,\bar{6}2'). \end{aligned} \tag{4.11}$$

In the case of the Hartree-Fock-Bogoliubov mean field approximations, the functional derivative $\left(\frac{\delta\Sigma(\bar{3},\bar{4})}{\delta G(5,6)}\right)_{\phi=0}$ is a combination of delta-functions

and no further Green's functions enter the equation. For translation invariant systems it is typically advantageous to rewrite this equation in momentum space.

The equation above can also be considered an implicit expansion and resummation in diagrams. The diagrammatic series is recovered by repeated nesting of the rigth hand side of Equation (4.11). Conversely, the linear response function can be derived using diagrammatic perturbation theory. Notice however that depending on the choice of diagrams for resummation, the diagrammatic derivation can lead to a result which is not self-consistent. In the case of the Hartree-Fock-Bogoliubov theory, the result of the self-consistent approach above is equivalent to the generalized random phase approximation (GRPA) [81].

The linear response function can be given two slightly different physical interpretations. On the one hand, it can be used to describe the time-evolution of the system under a specific perturbation, as is the case in the following section on the spin-asymmetric Josephson effect. On the other hand, one can find from the linear response function all possible single particle transitions of the system. Moreover, it is possible that the for some specific perturbations the linear response function diverges, formally implying that for a vanishingly small perturbation strength the system can have a non-trivial time-evolution. Such a resonance is in fact a signal of a collective excitation in the system. Therefore, in the frequency space, the poles of the linear response function can be interpreted as the collective excitation spectrum of the system. Thus, the response function contains information about the excitation spectrum of the system at equilibrium. This point of view can be taken with the results of Section 4.2 concerning the collective mode spectrum of the FFLO state.

4.1 Spin-asymmetric Josephson effect

The Josephson effect is a coherent tunneling phenomenon between two superconductors or superfluids. The Josephson effect can be divided to a direct current (DC) effect in which a finite supercurrent flows through the system at zero voltage, and an alternating current (AC) effect in which a constant voltage gives rise to an alternating current at a precisely defined Josephson frequency [82].

In the following, we discuss the spin-asymmetric Josephson effect, in which the two spin-components forming a Cooper pair are subjected to

different potentials [83]. This study is motivated by the possibility of having spin-dependent potentials in a quantum gas analogue of a Josephson junction. In fact, there are many different possibilities of creating such an experimental setup. In Publication I, our main focus was on a setup in which two superfluid Fermi gases are connected by a radio frequency (RF) fields. We will use this notation in the equations below. The formalism translates directly to the case of another possible experimental setup, a spin-dependent double well. In Publication IV we showed that also a spin-dependent superlattice can be used to produce the effect, and we return to this case after the introduction of the key features of the Josephson effect.

In the RF coupling case, the basic system is a four component Fermi gas in which the spin-states $|1\rangle$ and $|2\rangle$ form a BCS superfluid, as do the spin-states $|3\rangle$ and $|4\rangle$. The unperturbed Hamiltonian H_0 of the system is

$$H_0 = \int d\mathbf{r} \sum_i \psi_i^\dagger(\mathbf{r}) \left(-\frac{\nabla^2}{2m} - \mu_i \right) \psi_i(\mathbf{r}) + \frac{1}{2} \int d\mathbf{r} \sum_{i \neq j} U_{ij} \psi_i^\dagger(\mathbf{r}) \psi_j^\dagger(\mathbf{r}) \psi_j(\mathbf{r}) \psi_i(\mathbf{r}). \tag{4.12}$$

Here, we assume equal chemical potentials for all states $\mu_i \equiv \mu$, and furthermore, equal interaction strength for the paired states, i.e. $U_{12} = U_{34}$, whence the resulting two BCS states are identical. We then introduce a RF coupling between states $|1\rangle$ and $|3\rangle$, as well as between states $|3\rangle$ and $|4\rangle$. The tunneling coupling between states $|i\rangle$ and $|j\rangle$ can be described in the rotating wave approximation [84], and is characterized by the Rabi frequency Ω_{ij} and the detuning $\delta_{ij} = \nu_{ij} - \omega_{ij}$. Here ν_{ij} and ω_{ij} are the frequencies of the RF field and the atomic transition, respectively. The Hamiltonian of the RF coupling is

$$\begin{aligned} H_{RF} = & \frac{\delta_{13}}{2} \int d\mathbf{r} (\psi_1^\dagger(\mathbf{r}) \psi_1(\mathbf{r}) - \psi_3^\dagger(\mathbf{r}) \psi_3(\mathbf{r})) \\ & + \frac{\delta_{24}}{2} \int d\mathbf{r} (\psi_2^\dagger(\mathbf{r}) \psi_2(\mathbf{r}) - \psi_4^\dagger(\mathbf{r}) \psi_4(\mathbf{r})) \\ & + \Omega_{13} \int d\mathbf{r}\, \psi_1^\dagger(\mathbf{r}) \psi_3(\mathbf{r}) + h.c. + \Omega_{24} \int d\mathbf{r}\, \psi_2^\dagger(\mathbf{r}) \psi_4(\mathbf{r}) + h.c. \end{aligned} \tag{4.13}$$

In the case of a double well (with labels left and right assigned to the two wells) the states $|1\rangle$ and $|2\rangle$ would correspond to the spin up and spin down fermions in the left well, and states $|3\rangle$ and $|4\rangle$ to the spin up and spin down fermions in the right well. The detunings δ_{13} and δ_{24} would then be the spin-dependent potential differences between the two wells. A more detailed description of these two setups is given in Publication I. Note that if the time-dependence of the original electromagnetic field

is defined as a sine-wave, and not a complex exponential, an additional factor of one half has to be added to the Rabi frequency terms.

Let us define the current as $I_\sigma(t) \equiv \langle \dot{N}_\sigma \rangle$. Following the standard derivation of the Josephson effect [85, 86, 87], which is essentially the derivation of the Kubo formula with the time-dependence of the supercurrent taken as a prefactor, the current $I_1(t)$ becomes

$$\begin{aligned} I_1(t) &= I_1^S + I_1^J(t) \\ I_1^S(t) &= -2\Omega_{13}^2 \mathrm{Im}\left(L_{1331}(\mathbf{p}=0, \delta_{13} + i\eta^+)\right), \\ I_1^J(t) &= 2\Omega_{13}\Omega_{24}|L_{1234}(\mathbf{p}=0, -\delta_{24} + i\eta^+)| \sin[(\delta_{13}+\delta_{24})t + \varphi]. \end{aligned} \tag{4.14}$$

The term I_1^S in the equation above is the normal (or dissipative) current. In the following discussion we assume that the temperature is zero and that the detunings are smaller than the BCS gap, $|\delta| < 2\Delta$, in which case I^S is zero. The term I_1^J is the Josephson current and its amplitude defines the critical current $I_{13}^C(\delta_{24})$. Thus, the Josephson current for each spin-component is

$$\begin{aligned} I_1^J(t) &= I_1^C(\delta_{24}) \sin[(\delta_{13}+\delta_{24})t + \varphi], \\ I_2^J(t) &= I_2^C(\delta_{13}) \sin[(\delta_{13}+\delta_{24})t + \varphi], \\ I_1^C(\delta_{24}) &= 2\Omega_{13}\Omega_{24}|L_{1234}(\mathbf{p}=0, -\delta_{24} + i\eta^+)|, \\ I_2^C(\delta_{13}) &= 2\Omega_{13}\Omega_{24}|L_{2143}(\mathbf{p}=0, -\delta_{13} + i\eta^+)|. \end{aligned} \tag{4.15}$$

In Publication I, the linear response functions above were solved self-consistently in a general case when the two superfluids are interacting, as would be appropriate in the RF-frequency setup. There, it was shown that while the interactions modify the result quantitatively, the qualitative picture of the spin-asymmetric Josephson effect remains the same. Thus, in the following discussion we may assume that there are no direct interactions between the two superfluids. In this case, the critical current I_{13}^C is the same function as I_{24}^C, and their only difference is in their dependence on the detunings.

Figure 4.1 demonstrates the main features of the result. The magnitude of the critical current for each spin component can be tuned independently with the choice of the detuning. However, the Josephson frequency is the same for both the spin components, $\delta_{13} + \delta_{24}$. Thus, the Josephson currents of the spin components oscillate at the same frequency, but with different amplitudes. The conventional interpretation of the Josephson effect is that it is caused by the coherent tunneling of Cooper pairs. This picture of pair tunneling seems to be in complete contradiction with the

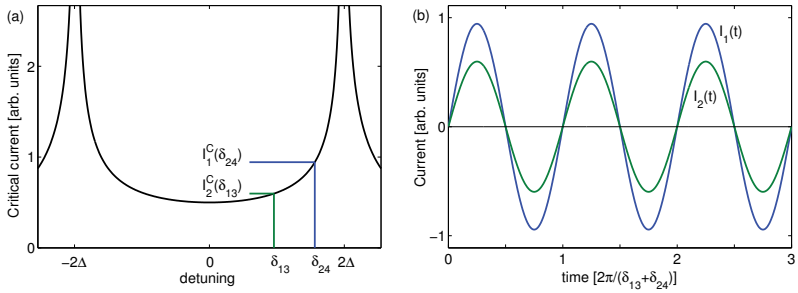

Figure 4.1. (a) The critical Josephson current as a function of the detuning. The critical current of each spin-component can be tuned individually with the choice of the detunings. The critical current diverges when the detuning is equal to 2Δ, where Δ is the superfluid gap. This structure is known as the Riedel peak. (b) The current of each spin-component oscillates at the Josephson frequency $\delta_{13} + \delta_{24}$. However, when $\delta_{13} \neq \delta_{24}$, the amplitudes of the currents are different, suggesting that there is more to the Josephson effect than just the tunneling of Cooper pairs. Figure (a) adapted from Publication I.

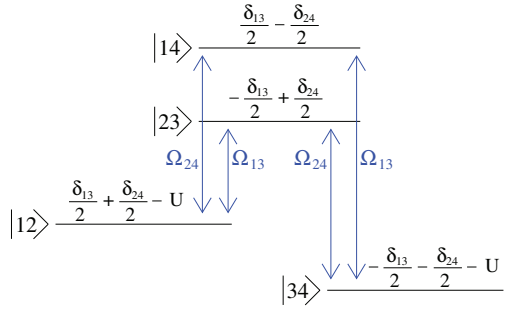

Figure 4.2. The level diagram of the four-state system, which can be used as the simplest possible model system for the spin-asymmetric Josephson effect. The parameter U is the energy gained by pairing. Figure originally published in Publication I.

spin-asymmetric result. In fact, it turns out that the resolution of this intriguing paradox leads to a new interpretation of the entire Josephon effect, as first discussed in Publication I.

The initial state of the system is a product of two BCS states

$$\begin{aligned} |\Psi\rangle &= |\mathrm{BCS}\rangle_{12} \otimes |\mathrm{BCS}\rangle_{34} \\ &= \prod_k \left(u_k + v_k \hat{c}^\dagger_{1,k} \hat{c}^\dagger_{2,-k}\right) \prod_{k'} \left(u_{k'} + v_{k'} \hat{c}^\dagger_{3,k'} \hat{c}^\dagger_{4,-k'}\right) |\emptyset\rangle \,. \end{aligned} \tag{4.16}$$

Let us simplify the situation by focusing on a single momentum state k:

$$\begin{aligned} |\Psi_k\rangle &= (u_k + v_k \hat{c}^\dagger_{1,k} \hat{c}^\dagger_{2,-k})(u_k + v_k \hat{c}^\dagger_{3,k} \hat{c}^\dagger_{4,-k}) \, |\emptyset\rangle \\ &= u_k^2 \, |\emptyset\rangle + v_k^2 \hat{c}^\dagger_{1,k} \hat{c}^\dagger_{2,-k} \hat{c}^\dagger_{3,k} \hat{c}^\dagger_{4,-k} \, |\emptyset\rangle + u_k v_k \left(\hat{c}^\dagger_{1,k} \hat{c}^\dagger_{2,-k} + \hat{c}^\dagger_{3,k} \hat{c}^\dagger_{4,-k}\right) |\emptyset\rangle \,. \end{aligned} \tag{4.17}$$

The empty state and the completely filled state cannot contribute to the

current, and therefore, the dynamics of the system follows from the initial superposition of the states $|12\rangle = \hat{c}^\dagger_{1,k}\hat{c}^\dagger_{2,-k}|\emptyset\rangle$ and $|34\rangle = \hat{c}^\dagger_{3,k}\hat{c}^\dagger_{4,-k}|\emptyset\rangle$. Now, the tunneling matrix elements couple these states through single particle transitions, and therefore the description of the dynamics must also inlude the states $|14\rangle = \hat{c}^\dagger_{1,k}\hat{c}^\dagger_{4,-k}|\emptyset\rangle$ and $|23\rangle = \hat{c}^\dagger_{2,-k}\hat{c}^\dagger_{3,k}|\emptyset\rangle$ which are analogous to single particle excitations within the BCS formalism.

The resulting four level system is described in Figure 4.2. Solving the time-evolution of this system to second order in the tunneling matrix element we find the following current for $\sigma = 1$ at the Josephson frequency

$$I_1^J = 2\Omega_{13}\Omega_{24}\left(M_{\mathrm{pair}} + M_{\mathrm{single}}\right)\sin[(\delta_{13} + \delta_{24})t] \tag{4.18}$$

Here, we have grouped the various terms in the perturbation expansion to two coefficients, M_{pair} and M_{single}. The term M_{pair} is given by

$$M_{\mathrm{pair}} = \frac{1}{U + \delta_{13}} + \frac{1}{U + \delta_{24}}, \tag{4.19}$$

where the pairing energy is denoted by U. This term arises from the second order tunneling processes which start from the paired state $|34\rangle$, pass through either one of the broken pair states $|14\rangle$ or $|23\rangle$, and end in the state $|12\rangle$, i.e. the pair interference processes. The term is symmetric in the detunings and an identical term is found in the current of the second spin component I_2^J.

The term M_{single} is defined as

$$M_{\mathrm{single}} = \frac{1}{U - \delta_{24}} - \frac{1}{U + \delta_{13}}. \tag{4.20}$$

This contribution corresponds to interference on state $|14\rangle$ and was first identified in Publication I. In other words, this is an interference term of two first order tunneling processes in which a paired state is broken, i.e. $|12\rangle \rightarrow |14\rangle$ and $|34\rangle \rightarrow |14\rangle$. This interference of broken pairs explains the asymmetry of the Josephson current, since the corresponding contribution to I_2^J originates from state $|23\rangle$ and is of the form

$$\tilde{M}_{\mathrm{single}} = \frac{1}{U - \delta_{13}} - \frac{1}{U + \delta_{24}}. \tag{4.21}$$

Thus, the spin-asymmetric Josephson effect is ultimately caused by the fact that the spin-asymmteric potential leads to an energy difference between the intermediate states $|14\rangle$ and $|23\rangle$. The many-body result can be recovered from the four-state formulation by summing over the momentum with the appropriate pre-factors from the BCS ansatz. Here, one notices the importance of the phase coherence in the initial state; all

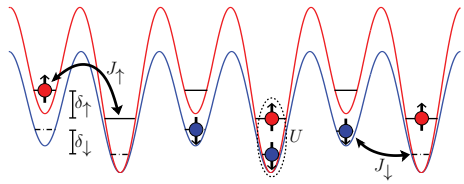

Figure 4.3. When a spin-dependent superlattice potential is imposed on a regular optical lattice, the spin-asymmetric Josephson effect occurs between the odd and even lattice sites. In this configuration, each pair of adjacent lattice sites can be compared to a small Josephson junction. Figure originally published in Publication IV.

of the four-state systems corresponding to differenct momenta have the same initial condition. Moreover, the Josephson frequency is the same for all sub-systems. Notice, that for a momentum conserving tunneling matrix such as the RF coupling, the four-state picture holds exactly to all orders of perturbation theory, whereas in the case of a general tunneling matrix, it is valid to the second order in perturbation theory, as shown in Publication IV.

The discussion above suggests that the Josephson effect in general can be interpreted as Rabi oscillations in a four-state system. Now, the interesting point here is that the broken pair interference term above is present, and equally important as the pair tunneling term, also in the case of the conventional Josephson effect with no spin-dependence, i.e. $\delta_{13} = \delta_{24}$. Therefore, the interpretation of the Josephson effect as tunneling of Cooper pairs is insufficient.

In Publication IV we considered an alternate approach to the experimental realization of the Josephson effect using a spin-dependent superlattice, see Figure 4.3. Here, the Josephson effect occurs in fact within one single superfluid, between the odd and even sites of the superlattice. Also in this configuration, the individual control of the potentials for each spin component leads to the spin-asymmetric Josephson effect, as we demonstrated utilizing the time-evolving block decimation (TEBD) algorithm for essentially exact simulations of the dynamics of the system. However, we also showed that in the superlattice system there are subtle differences to the standard Josephson effect. The hopping, which in this setup is the equivalent of the tunneling coupling between the two superfluids, is typically comparable to the other energy scales in the system, and there are corrections to the second order perturbation theory results: The Josephson frequency is shifted from its weak-coupling limit value $\delta_{13} + \delta_{24}$ and is

split to several adjacent frequencies.

Finally, in Publication IV we discussed the connection of the spin-asymmetric Josephson effect to various solid-state Josephson junction configurations. Here, the limiting case of the DC Josephson effect is of particular interest. In the spin-asymmetric case, the DC limit is given by the condition of zero Josephson frequency, $\delta_{13} + \delta_{24} = 0$. Now, this condition leaves undetermined one degree of freedom, $\delta = |\delta_{13}| = |\delta_{24}|$, which affects the critical Josephson current. Therefore, we find that the critical DC current can be tuned by having opposite, but non-zero detunings. In fact, this leads to the enhancement of the critical current, as is evident from Figure 4.1, since the spin-symmetric case corresponds to $\delta = 0$. A similar enhancement has been predicted to occur in a Josephson junction with a specific ferromagnetic layer structure, the SFIFS junction, where S, F and I stand for superconducting, ferromagnetic and insulating layers [88, 89]. Here, a key assumption of the SFIFS junction is that it is short in the sense that the SF-bilayer can be considered a uniform magnetic superconductor, whereas in the opposite limit of a long junction, the system demonstrates a different behavior [90]. In Publication IV we show that the enhancement of the critical current is analogous to the tunable DC effect and explain the origin of this effect in terms of the formalism outlined above.

4.2 Collective modes in the Fulde-Ferrell-Larkin-Ovchinnikov (FFLO) state

The FFLO state demonstrates a very peculiar form of symmetry breaking. In the FFLO state, the order parameter has a preferred direction, and the state is therefore anisotropic. Thus, it is interesting to ask whether this anisotropy would leave its mark on the response properties and the collective mode spectrum of the system. Moreover, the interplay of the Cooper pairs and the substantial number of unpaired particles may also have important consequences to these properties. These questions were studied in Publication II in the case of the plane wave order parameter.

The mean-field approximation for the FFLO state was described in detail in Section 3.1 and provides the starting point for the derivation of the self-consistent FFLO density response function. Now, the density response function is of the form $\chi_1(\mathbf{k}, \omega) = L_{1111}(\mathbf{k}, \omega) + L_{1212}(\mathbf{k}, \omega)$ where L_{1111} and L_{1212} are the linear response functions of density n_1 to the po-

tentials ϕ_1 and ϕ_2, which are typically assumed equal in strength. As discussed in the beginning of this chapter the collective modes of the system appear as the poles of the density response function. The general self-consistent formalism presented above can be followed to obtain the response functions L_{1111} and L_{1212}. The non-trivial step of the derivation is again, as in Section 3.1, the transformation to momentum basis with proper treatment of the FFLO pairing momentum $\mathbf{q}$. In the momentum basis, the problem separates after some algebra to a block-diagonal form, where each block contains two momenta connected by the FFLO pairing momentum. When symmetries with respect to the spin-index are taken into account, each momentum block can be reduced to the following 4×4 matrix equation. The following result was derived in Publication II.

The linear response function L_{1111} is obtained from the equation

$$L^{(1)}(\mathbf{p}_1, \mathbf{p}_2) = \delta_{\mathbf{p}_1,\mathbf{p}_2}[M^{(1)}(\mathbf{p}_1)]^{-1}\Pi^{(1)}(\mathbf{p}_1). \tag{4.22}$$

Here, all the quantities are have the same Matsubara frequency ω. The vector of linear response functions, $L^{(1)}$, is defined as

$$L^{(1)}(\mathbf{p}_1, \mathbf{p}_2) = \\ \Big[L_{1111}(\mathbf{p}_1, \mathbf{p}_2) \quad L_{1141}(2\mathbf{q} + \mathbf{p}_1, -\mathbf{p}_2) \quad L_{4111}(2\mathbf{q} - \mathbf{p}_1, \mathbf{p}_2) \quad L_{4141}(-\mathbf{p}_1, -\mathbf{p}_2)\Big]^T, \tag{4.23}$$

while $\Pi^{(1)}$ is

$$\Pi^{(1)}(\mathbf{p}_1) = \Big[\Pi_{1111}(\mathbf{p}_1) \quad \Pi_{1114}(\mathbf{p}_1) \quad \Pi_{4111}(\mathbf{p}_1) \quad \Pi_{4114}(\mathbf{p}_1)\Big]^T. \tag{4.24}$$

Here, we have defined $\Pi_{\sigma_1\sigma_2\sigma_3\sigma_4}(\mathbf{p}_1)$ as

$$\begin{aligned}\Pi_{\sigma_1\sigma_2\sigma_3\sigma_4}(\mathbf{p}, \omega) =& \frac{1}{\beta N_L}\sum_{\mathbf{s},\chi} G_{\sigma_1\sigma_2}(\lambda_{\sigma_1}(\mathbf{p}+\mathbf{s}), \lambda_{\sigma_2}(\mathbf{p}+\mathbf{s}), \chi+\omega) \\ & \times G_{\sigma_3\sigma_4}(\lambda_{\sigma_3}(\mathbf{s}), \lambda_{\sigma_4}(\mathbf{s}), \chi),\end{aligned} \tag{4.25}$$

where N_L is the number of lattice sites and $\lambda_\sigma(\mathbf{p})$ is defined so that

$$\lambda_\sigma(\mathbf{p}) = \mathbf{p}, \quad \sigma \in \{1, 2\}, \qquad \lambda_\sigma(\mathbf{p}) = 2\mathbf{q} - \mathbf{p}, \quad \sigma \in \{3, 4\}. \tag{4.26}$$

The matrix $M^{(1)}$ is

$$M^{(1)}(\mathbf{p}_1) = I - U \begin{bmatrix} -\Pi_{1441}(\mathbf{p}_1) & \Pi_{1141}(\mathbf{p}_1) & \Pi_{1411}(\mathbf{p}_1) & -\Pi_{1111}(\mathbf{p}_1) \\ -\Pi_{1444}(\mathbf{p}_1) & \Pi_{1144}(\mathbf{p}_1) & \Pi_{1414}(\mathbf{p}_1) & -\Pi_{1114}(\mathbf{p}_1) \\ -\Pi_{4441}(\mathbf{p}_1) & \Pi_{4141}(\mathbf{p}_1) & \Pi_{4411}(\mathbf{p}_1) & -\Pi_{4111}(\mathbf{p}_1) \\ -\Pi_{4444}(\mathbf{p}_1) & \Pi_{4144}(\mathbf{p}_1) & \Pi_{4414}(\mathbf{p}_1) & -\Pi_{4114}(\mathbf{p}_1) \end{bmatrix}. \tag{4.27}$$

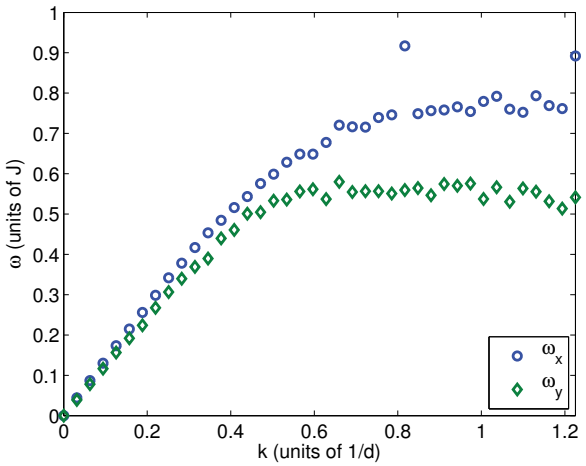

Figure 4.4. The dispersion relation of the collective density modes in the FFLO state when the wave vector is parallel to the the FFLO vector $\mathbf{q}$ (ω_x), and perpendicular to it (ω_y). The speed of sound is given by the slope of the dispersion at $k = 0$. The anisotropic nature of the FFLO state leads to an anisotropy in the speed of sound. Figure originally published in Publication II.

One derives similarly for L_{1212} the equation

$$L^{(2)}(\mathbf{p}_1, \mathbf{p}_2) = -\delta_{\mathbf{p}_1,\mathbf{p}_2}[M^{(2)}(\mathbf{p}_1)]^{-1}\Pi^{(2)}(\mathbf{p}_1), \tag{4.28}$$

where $L^{(2)}$ is given by

$$L^{(2)}(\mathbf{p}_1, \mathbf{p}_2) = \\ \Big[L_{1212}(\mathbf{p}_1, \mathbf{p}_2) \quad L_{1242}(2\mathbf{q} + \mathbf{p}_1, -\mathbf{p}_2) \quad L_{4212}(2\mathbf{q} - \mathbf{p}_1, \mathbf{p}_2) \quad L_{4242}(-\mathbf{p}_1, -\mathbf{p}_2)\Big]^T, \tag{4.29}$$

and $\Pi^{(2)}$ is

$$\Pi^{(2)}(\mathbf{p}_1) = \Big[\Pi_{1441}(\mathbf{p}_1) \quad \Pi_{1444}(\mathbf{p}_1) \quad \Pi_{4441}(\mathbf{p}_1) \quad \Pi_{4444}(\mathbf{p}_1)\Big]^T. \tag{4.30}$$

The matrix $M^{(2)}$ is the same as $M^{(1)}$. This implies that the same collective mode spectrum would be found in either of the response functions L_{1111} and L_{1212}, or indeed their sum $\chi_1(\mathbf{k}, \omega)$. Notice though that the non-resonant, or finite, values of these response functions are in general different.

In Publication II this set of equations was solved numerically. The analytical continuation of the response function was carried out using a Padé approximant in a form described in [91]. This approach was particularly useful in that it allowed the solution of the real and imaginary parts of the poles of the response function, i.e. the collective mode resonance frequency and the damping rate, on equal footing. The main result presented

in Publication II was that the collective mode dispersion in the FFLO state depends on the direction relative to the FFLO vector as shown in Figure 4.4. Since this collective mode is soundlike, i.e. gapless and linear at the long wave length limit, the result can be summarized by the fact that the speed of sound in the FFLO state is anisotropic. The analysis of the damping rate indicated that the collective mode is well-defined in the sense that the damping rate is small compared to the mode frequency.

The GRPA formalism has also been utilized for the case of a 1D Fermi gas in the LO state in reference [92, 93], where a density response with two collective mode branches was reported. Similar results have been found for the LO state also in higher dimensions using a Ginzburg-Landau model [94]. Interstingly, in Publication II we showed that a very similar response function arises also in the case of the FF ansatz in a quasi-1D geometry, since the response of the unpaired quasiparticles is restricted to a very narrow momentum band when the dimensionality is reduced. Finally, the back-bending of the collective mode dispersion at large momenta in 2D and 3D systems has been interpreted as roton-like behavior [95, 96].

4.2.1 Connection to the Goldstone theorem

The Goldstone theorem states that the spontaneous breaking of a global continuous symmetry results in a Nambu-Goldstone mode, which is a bosonic excitation of the ground state with a gapless dispersion at the long wave length limit [97]. The crude explanation for this is that a long wave length transformation of the order parameter can smoothly interpolate between different possible ground state values of the order parameter, all equally optimal in the free energy.

The collective mode discussed in the preceding section is known as the Anderson-Bogoliubov phonon in the case of the BCS state. The Anderson-Bogoliubov phonon can be interpreted as the Nambu-Goldstone mode related to the spontaneous symmetry breaking of the phase of the superfluid order parameter. Here, an essential point is that the Anderson-Bogoliubov phonon occurs in a neutral system, such as a superfluid quantum gas. However, in a charged system, i.e. a superconductor, a notable exception occurs. In this case, we have in fact a local symmetry breaking of the gauge field. The condensate phase is coupled to the vector potential which absorbs the Goldstone mode, and as a result, the collective mode spectrum of the system is gapped (or massive). This is an example of the

famous Higgs mechanism.[1]

In the following, we give a detailed analytical proof that the collective mode predicted for the FFLO state using the GRPA formalism is gapless, and as a result, the physical picture is consistent with the Goldstone theorem. Technically, we show that the linear response function of Equation (4.22) diverges at the limit of zero momentum and energy ($\mathbf{p} = 0, \omega = 0$), or in other words, we show that the matrix $M^{(1)}$ of Equation (4.27) is singular at this limit. Technically, we show that the determinant of $M^{(1)}$ is zero in this limit. In fact, we shall see that the crucial step in the proof is to identify that the gap equation (3.23) is self-consistently included to this matrix.

We begin by calculating the general term $\Pi_{abcd}(\mathbf{p}, \omega)$ in the limit $\mathbf{p} = 0, \omega = 0$. We take the limit $\mathbf{p} = 0$ at the very beginning of the calculation but postpone taking the limit $\omega = 0$. The Green's functions of the matrix block $a, b \in \{1, 4\}$ are needed for $\mathbf{p}_1 = \mathbf{p}_2 = \mathbf{s}$, and for the calculation ahead we restate the FFLO Green's functions of Equation (3.19) in the form

$$G_{ab}(\lambda_a(\mathbf{s}), \lambda_b(\mathbf{s}), \omega) = \frac{X_{ab}(\mathbf{s})}{i\omega - E_+(\mathbf{s})} + \frac{Y_{ab}(\mathbf{s})}{i\omega + E_-(\mathbf{s})}. \tag{4.31}$$

From here on we simplify the notation by leaving out the momentum variable s from the terms in the sum. The term $\Pi_{abcd}(\mathbf{p} = 0, \omega)$ is

$$\begin{aligned}
\Pi_{abcd}(\mathbf{p} = 0, \omega) &= \frac{1}{\beta N_L} \sum_{\chi, \mathbf{s}} G_{ab}(\omega + \chi) G_{cd}(\chi) \\
&= \frac{1}{\beta N_L} \sum_{\chi, \mathbf{s}} \frac{X_{ab} X_{cd}}{(i\omega + i\chi - E_+)(i\chi - E_+)} + \frac{X_{ab} Y_{cd}}{(i\omega + i\chi - E_+)(i\chi + E_-)} \\
&+ \frac{Y_{ab} X_{cd}}{(i\omega + i\chi + E_-)(i\chi - E_+)} + \frac{Y_{ab} Y_{cd}}{(i\omega + i\chi + E_-)(i\chi + E_-)}.
\end{aligned} \tag{4.32}$$

The general Matsubara sum in the equation above is evaluated as [74, 75, 76]

$$\frac{1}{\beta} \sum_{\chi} \frac{1}{i(\omega + \chi) - E_1} \cdot \frac{1}{i\chi - E_2} = \frac{n_F(E_1) - n_F(E_2)}{E_1 - E_2 - i\omega}. \tag{4.33}$$

Noticing that the first and fourth terms of Equation (4.32) vanish identically, and taking into account that $n_F(-x) = 1 - n_F(x)$, we find

$$\begin{aligned}
\Pi_{abcd}(\mathbf{p} = 0, \omega) = -\frac{1}{N_L} \sum_{\mathbf{s}} &\frac{X_{ab} Y_{cd} (1 - n_F(E_+) - n_F(E_-))}{E_+ + E_- - i\omega} \\
&+ \frac{Y_{ab} X_{cd} (1 - n_F(E_-) - n_F(E_+))}{E_- + E_+ + i\omega}.
\end{aligned} \tag{4.34}$$

[1] In both the neutral and the charged system, there can also exist a gapped mode related to the oscillation of the amplitude of the order parameter. This is referred to as the amplitude mode or the Higgs mode.

We may now carry out the analytical continuation to real frequencies via the substitution $i\omega \to \omega + i0^+$ and the identity $\frac{1}{x-i0^+} = P\frac{1}{x} + i\pi\delta(x)$. Since $E_+ + E_- > 2\Delta$, the analytical continuation yields for $|\omega| < 2\Delta$ only the principal value with no imaginary part which would be proportional to a delta function of $E_+ + E_- - \omega$ in the first term and of $E_+ + E_- + \omega$ in the second one. Finally, upon taking the limit $\omega = 0$ we have

$$\Pi_{abcd}(\mathbf{p} = 0, \omega = 0) = -\frac{1}{N_L}\sum_{\mathbf{s}}(X_{ab}Y_{cd} + Y_{ab}X_{cd})\frac{(1 - n_F(E_+) - n_F(E_-))}{E_+ + E_-}. \tag{4.35}$$

Since $E_+ + E_- = \Delta/(uv)$ this can be rewritten as

$$\Pi_{abcd} = -\frac{1}{\Delta N_L}\sum_{\mathbf{s}} uv(X_{ab}Y_{cd} + Y_{ab}X_{cd})(1 - n_F(E_+) - n_F(E_-)). \tag{4.36}$$

The insertion of the FFLO Green's functions of Equation (3.19) to Equation (4.36) yields the following identities which are needed to complete the derivation.

$$\begin{aligned}
\Pi_{1144} &= -\frac{1}{\Delta N_L}\sum_{\mathbf{s}} uv(u^4 + v^4)(1 - n_F(E_+) - n_F(E_-)),\\
\Pi_{1414} &= -\frac{1}{\Delta N_L}\sum_{\mathbf{s}} uv(-2u^2v^2)(1 - n_F(E_+) - n_F(E_-)),\\
\Pi_{1141} = \Pi_{1411} &= -\frac{1}{\Delta N_L}\sum_{\mathbf{s}} uv(-u^3v + uv^3)(1 - n_F(E_+) - n_F(E_-)).
\end{aligned} \tag{4.37}$$

One shows similarly to above that $\Pi_{4144} = \Pi_{4414}$.

Now, we are ready to show that the determinant of $M^{(1)}$ is zero for $\mathbf{p} = 0, \omega = 0$. Recall that the value of a determinant is invariant under the operation of subtracting a single matrix column from any other column. Subtracting the third column of $M^{(1)}$ from the second column, we have

$$|M^{(1)}| = \begin{vmatrix}
1 + U\Pi_{1441} & -U\Pi_{1141} + U\Pi_{1411} & -U\Pi_{1411} & U\Pi_{1111}\\
U\Pi_{1444} & 1 - U\Pi_{1144} + U\Pi_{1414} & -U\Pi_{1414} & U\Pi_{1114}\\
U\Pi_{4441} & -U\Pi_{4141} + U\Pi_{4411} - 1 & 1 - U\Pi_{4411} & U\Pi_{4111}\\
U\Pi_{4444} & -U\Pi_{4144} + U\Pi_{4414} & -U\Pi_{4414} & 1 + U\Pi_{4114}
\end{vmatrix}. \tag{4.38}$$

Now, on the second column the first and fourth terms vanish as we have concluded that $\Pi_{1141} = \Pi_{1411}$ and $\Pi_{4144} = \Pi_{4414}$. The second term in the

second column is

$$\begin{aligned} 1 - U\Pi_{1144} + U\Pi_{1414} &= 1 + \frac{U}{\Delta N_L}\sum_{\mathbf{s}} uv(u^4 + v^4 + 2u^2v^2)(1 - n_F(E_+) - n_F(E_-)) \\ &= 1 + \frac{U}{\Delta N_L}\sum_{\mathbf{s}} uv(u^2 + v^2)^2(1 - n_F(E_+) - n_F(E_-)) \\ &= 1 + \frac{U}{\Delta N_L}\sum_{\mathbf{s}} uv(1 - n_F(E_+) - n_F(E_-)) \\ &= 0. \end{aligned} \tag{4.39}$$

The last equality above follows directly from the gap equation (3.23). One shows similarly that because of the gap equation the third term of the second column vanishes, and as a result we finally obtain

$$|M^{(1)}| = \begin{vmatrix} 1 + U\Pi_{1441} & 0 & -U\Pi_{1411} & U\Pi_{1111} \\ U\Pi_{1444} & 0 & -U\Pi_{1414} & U\Pi_{1114} \\ U\Pi_{4441} & 0 & 1 - U\Pi_{4411} & U\Pi_{4111} \\ U\Pi_{4444} & 0 & -U\Pi_{4414} & 1 + U\Pi_{4114} \end{vmatrix} = 0. \tag{4.40}$$

We have now shown that the matrix $M^{(1)}$ is singular for $\mathbf{q} = 0, \omega = 0$. Firstly, this means that the collective mode is gapless. Secondly, this occurs precisely because of the fact that the gap equation is included consistently into the formalism of calculating the collective mode spectrum. Consequently, the collective mode described by the formalism can be identified as the Nambu-Goldstone mode of the FFLO state.

5. Dynamical mean-field theory

Dynamical mean-field theory (DMFT) [98] is a widely used framework for solving quantum many-body problems on a lattice at thermodynamic equilibrium. DMFT is non-perturbative, and therefore, it can be applied to strongly correlated systems. Arguably the most renowned example of the power of DMFT is the correct description of the Mott insulating transition. While the method was originally conceived for fermions, recently it has been implemented for bosonic systems as well [99, 100]. Here, we will keep with the main theme of this thesis and focus on fermions.

The main idea of DMFT is a self-consistent mapping of the many-body problem to a quantum impurity problem as described in Figure 5.1. In the construction of this mapping it is assumed that the self-energy of the system is local

$$\Sigma_{jl}(i\omega_n) \approx \delta_{jl}\Sigma_j(i\omega_n). \tag{5.1}$$

DMFT effectively splits the original problem to two halves, solving the lattice Dyson equation for a given self-energy and solving a quantum impurity problem for a given mapping. Though the impurity problem is computationally far more tractable than the full problem, it is still a demanding quantum many-body problem in its own right, and in general, sophisticated numerical techniques are required for its solution. In Section 5.3 we discuss how the impurity problem can be solved. Before this, we introduce DMFT in more detail in Section 5.1 using real-space formalism [101, 102, 103, 104] which is relevant for spatially non-uniform systems such as quantum gases in a trap, and outline in Section 5.2 how cluster DMFT formalism can be utilized to find systematic corrections to the DMFT approximation. Finally, in Section 5.4 we present key results from our studies on spin-polarized superfluidity using these methods.

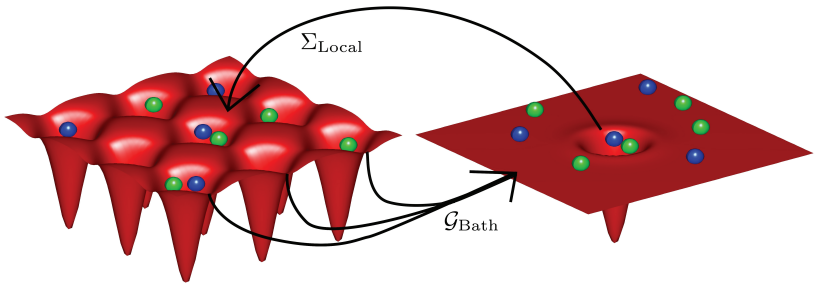

Figure 5.1. The concept of dynamical mean field theory (DMFT). The system is mapped to an impurity problem which has one lattice site with interaction. The rest of the system is represented as a bath of non-interacting particles which tunnel in and out of the chosen lattice site. The local self-energy can be solved from the impurity problem and fed back to the original lattice geometry. The physically correct solution satisfies a self-consistency condition, i.e. is represented by a self-energy which creates its own bath, and is found by means of fixed point iteration.

5.1 Real-space dynamical mean-field theory (DMFT)

The study of quantum gas systems motivates the formulation of the DMFT method in a way which accommodates spatially inhomogeneous systems. Our focus is also on the phenomenon of superfluidity. In order to describe the superfluid symmetry breaking, the anomalous pairing correlations need to be incorporated to DMFT, and the standard approach here is to utilize Nambu formalism. The Nambu Green's function is defined in a 2×2 block form as follows

$$\boldsymbol{G}_{ij} = \begin{bmatrix} G_{\uparrow,ij}(\tau) & F_{ij}(\tau) \\ F^{\dagger}_{ij}(\tau) & -G_{\downarrow,ji}(-\tau) \end{bmatrix} = \begin{bmatrix} -\left\langle T_\tau \hat{c}_{i,\uparrow}(\tau)\hat{c}^{\dagger}_{j,\uparrow}(0)\right\rangle & -\left\langle T_\tau \hat{c}_{i,\uparrow}(\tau)\hat{c}_{j,\downarrow}(0)\right\rangle \\ -\left\langle T_\tau \hat{c}^{\dagger}_{i,\downarrow}(\tau)\hat{c}^{\dagger}_{j,\uparrow}(0)\right\rangle & -\left\langle T_\tau \hat{c}^{\dagger}_{i,\downarrow}(\tau)\hat{c}_{j,\downarrow}(0)\right\rangle \end{bmatrix} \tag{5.2}$$

This is equivalent to the $\sigma = \{1, 4\}$ matrix block of Section 3.1. As the notation above suggests, we have $F^{\dagger}_{ij}(\tau) = [F_{ij}(\tau)]^{\dagger}$; note here that in Matsubara time-evolution we have $[\hat{O}(\tau)]^{\dagger} = \hat{O}^{\dagger}(-\tau)$. The self-energy of the system has the same block structure as the Green's function, while the non-interacting Green's function is given in Nambu formalism as follows

$$\boldsymbol{G}^{-1}_{0,ij}(i\omega_n) = \begin{bmatrix} i\omega_n + t_{ij} + (\mu_\uparrow - V_{i,\uparrow})\delta_{ij} & 0 \\ 0 & i\omega_n - t_{ij} - (\mu_\downarrow - V_{i,\downarrow})\delta_{ij} \end{bmatrix}. \tag{5.3}$$

Here, t_{ij} is the hopping and $V_{i,\sigma}$ the single-particle potential. Moreover, the order parameter of the superfluid phase is defined as

$$\Delta_i = -U\left\langle \hat{c}^{\dagger}_{i,\uparrow}\hat{c}^{\dagger}_{i,\downarrow}\right\rangle. \tag{5.4}$$

For a given self-energy, the Green's function can be defined through the

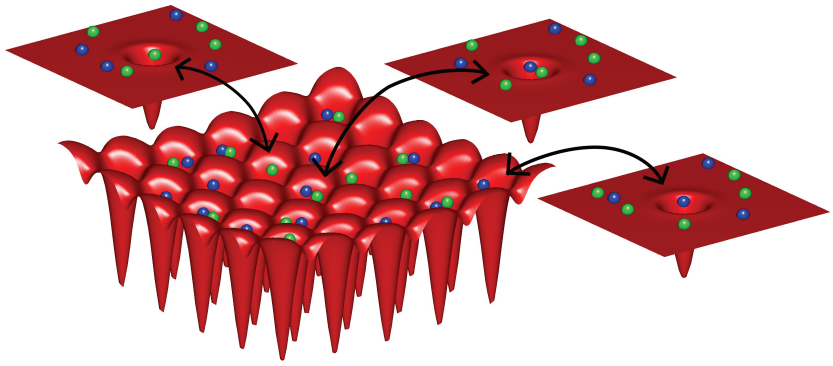

Figure 5.2. In real-space dynamical mean field theory a quantum impurity problem is solved for each lattice site in order to describe a spatially non-uniform system.

Dyson equation

$$\boldsymbol{G}_{jl}(i\omega_n) = [\boldsymbol{G}_0^{-1}(i\omega_n) - \boldsymbol{\Sigma}(i\omega_n)]^{-1}_{jl} \tag{5.5}$$

where in the case of DMFT the self-energy is site-diagonal, $\boldsymbol{\Sigma}_{jl}(i\omega_n) \approx \delta_{jl}\boldsymbol{\Sigma}_j(i\omega_n)$. In real-space DMFT the Dyson equation is solved directly via matrix inversion.

Let us now define the quantum impurity problem of lattice site j as the problem of solving the full local Green's function $\boldsymbol{\mathcal{G}}_j$ for the interaction strength U and a local bath Green's function $\boldsymbol{\mathcal{G}}_{\mathrm{Bath},j}$. In a diagrammatic expansion this is equivalent to the summation of all connected diagrams of $\boldsymbol{\mathcal{G}}_{\mathrm{Bath},j}$ and U.[1] For a given impurity problem, we may then calculate the local self-energy $\boldsymbol{\Sigma}_j(i\omega_n)$ from the Dyson equation

$$\boldsymbol{\Sigma}_{j,\sigma}(i\omega_n) = \boldsymbol{\mathcal{G}}^{-1}_{\mathrm{Bath},j}(i\omega_n) - \boldsymbol{\mathcal{G}}^{-1}_{j}(i\omega_n). \tag{5.6}$$

Now, the crucial point is how to connect the full lattice problem (5.5) to the quantum impurity problem (5.6). The connection is that the bath of the impurity problem is formed by removing the self-energy of site j from the local Green's function $\boldsymbol{G}_{jj}(i\omega_n)$. The bath Green's function is then defined by the equation

$$\boldsymbol{\mathcal{G}}^{-1}_{\mathrm{Bath},j}(i\omega_n) = [\boldsymbol{G}_{jj}(i\omega_n)]^{-1} + \boldsymbol{\Sigma}_j(i\omega_n). \tag{5.7}$$

Notice that on the right hand side of this equation we have specifically the inverse of the local component of $\boldsymbol{G}$ and not the jj-element of $\boldsymbol{G}^{-1}$. To

[1] The problem is of the same form as that of solving the Green's function G in a system of just one lattice site for a given non-interacting Green's function G_0 and the interaction strength U. In this case the local and global Green's functions are the same.

clarify the structure of the bath Green's function above, let us see explicitly what the removal of the local self-energy $\boldsymbol{\Sigma}_j$ means starting from the series expansion of the Dyson equation (5.5)

$$\begin{aligned}\boldsymbol{G}_{jl} &= \boldsymbol{G}_{0,jl} + \boldsymbol{G}_{0,jn_1}\boldsymbol{\Sigma}_{n_1n_2}\boldsymbol{G}_{0,n_2l} + \boldsymbol{G}_{0,jn_1}\boldsymbol{\Sigma}_{n_1n_2}\boldsymbol{G}_{0,n_2n_3}\boldsymbol{\Sigma}_{n_3n_4}\boldsymbol{G}_{0,n_4l} + \dots \\ &= \boldsymbol{G}_{0,jl} + \boldsymbol{G}_{0,jn_1}\boldsymbol{\Sigma}_{n_1}\boldsymbol{G}_{0,n_1l} + \boldsymbol{G}_{0,jn_1}\boldsymbol{\Sigma}_{n_1}\boldsymbol{G}_{0,n_1n_2}\boldsymbol{\Sigma}_{n_2}\boldsymbol{G}_{0,n_2l} + \dots \end{aligned} \tag{5.8}$$

Here, we have left out the Matsubara frequency for brevity and have an implied summation over repeated indices. On the second line, we have invoked the DMFT approximation of local self-energy. For the local problem at site j we then have

$$\boldsymbol{G}_{jj} = \boldsymbol{G}_{0,jj} + \boldsymbol{G}_{0,jn_1}\boldsymbol{\Sigma}_{n_1}\boldsymbol{G}_{0,n_1j} + \boldsymbol{G}_{0,jn_1}\boldsymbol{\Sigma}_{n_1}\boldsymbol{G}_{0,n_1n_2}\boldsymbol{\Sigma}_{n_2}\boldsymbol{G}_{0,n_2j} + \dots \tag{5.9}$$

Now, we can define the bath Green's function by removing the self-energy component $\boldsymbol{\Sigma}_j$ from every term of the series of $\boldsymbol{G}_{jj}$ above

$$\begin{aligned}\boldsymbol{\mathcal{G}}_{\mathrm{Bath},j} = \boldsymbol{G}_{0,jj} &+ \sum_{n_1\neq j} \boldsymbol{G}_{0,jn_1}\boldsymbol{\Sigma}_{n_1}\boldsymbol{G}_{0,n_1j} \\ &+ \sum_{n_1\neq j, n_2\neq j} \boldsymbol{G}_{0,jn_1}\boldsymbol{\Sigma}_{n_1}\boldsymbol{G}_{0,n_1n_2}\boldsymbol{\Sigma}_{n_2}\boldsymbol{G}_{0,n_2j} + \dots \end{aligned} \tag{5.10}$$

To see that this really is the bath Green's function of Equation (5.7), we re-write the series expansion of Equation (5.9) with the help of the bath Green's function defined above as

$$\begin{aligned}\boldsymbol{G}_{jj} &= \boldsymbol{\mathcal{G}}_{\mathrm{Bath},j} + \boldsymbol{\mathcal{G}}_{\mathrm{Bath},j}\boldsymbol{\Sigma}_j\boldsymbol{\mathcal{G}}_{\mathrm{Bath},j} + \boldsymbol{\mathcal{G}}_{\mathrm{Bath},j}\boldsymbol{\Sigma}_j\boldsymbol{\mathcal{G}}_{\mathrm{Bath},j}\boldsymbol{\Sigma}_j\boldsymbol{\mathcal{G}}_{\mathrm{Bath},j} + \dots \\ &= [\boldsymbol{\mathcal{G}}^{-1}_{\mathrm{Bath},j} - \boldsymbol{\Sigma}_j]^{-1}. \end{aligned} \tag{5.11}$$

The last expression above is equivalent to Equation (5.7). To conclude, the self-energy of all lattice sites aside for site j is included in the resulting bath Green's function, and thus, this object contains the information of how the interactions modify the non-interacting Green's function in all the other lattice sites.[2]

The physically correct solution to the equations above is defined by a self-consistency condition which is that the local Green's function $\boldsymbol{G}_{jj}(i\omega_n)$ and the impurity Green's function $\boldsymbol{\mathcal{G}}_j$ are equal. This is equivalent to finding a self-energy $\boldsymbol{\Sigma}_j(i\omega_n)$ which is the outcome of the impurity problem when given as input to the lattice Dyson Equation (5.5). The solution can be found by the means of a fixed point iteration starting from a given

[2]Notice that from the point of view of introducing DMFT in general, the Nambu formalism does not change the structure of the DMFT equations, and they can be readily interpreted as equations for the normal Green's function alone.

initial guess. We may then summarize the real-space DMFT algorithm as follows:

1. Guess the self-energy Σ_j.

2. Calculate the lattice Green's function from Equation (5.5).

3. Form the bath for the impurity problem of each lattice site from Equation (5.7).

4. Solve the impurity problem for each lattice site to obtain $\mathcal{G}_j$.

5. Compute new Σ_j from Equation (5.6).

6. Check for convergence: Finish if converged, else go to 2.

The bulk of the computational time is consumed in solving the impurity problem, but this part of the problem is parallelized efficiently, as each impurity problem can be solved independently. Notice that the lattice Dyson equation is diagonal in the Matsubara frequency, also allowing for a straightforward parallelization. Typically, the quantum Monte Carlo (QMC) solvers applicable to the impurity problem are implemented directly in terms of the bath Green's function, as explained in Section 5.3. However, for example the continuous-time auxiliary-field algorithm is formulated in complex time rather than Matsubara frequency space. Therefore, the initialization of the impurity problem requires a Fourier transformation from frequency space to complex time, and in this task, it is useful to take advantage of analytically soluble high frequency asymptotics [105].

The impurity problem can also be solved with methods other than QMC. For example it is possible to utilize exact diagonalization. In this case, the impurity problem has to be represented in a Hamiltonian form (with a finite number of orbitals), for instance using the Anderson impurity model. The parametrization of the impurity Hamiltonian is determined by a fit to the bath Green's function, and only after this additional step, the impurity problem itself can be solved.

There are two clear special cases where DMFT is exact. These are the non-interacting limit, and the atomic limit. In the non-interacting sys-

tem, the self-energy is identically zero. In the atomic limit defined by $J = 0$ or equivalently $|U| = \infty$ the system consists of isolated lattice sites, and therefore, the self-energy must be local as well. A slightly more non-trivial result is that the approximation $\mathbf{\Sigma}_{jl}(i\omega_n) = \delta_{jl}\mathbf{\Sigma}_j(i\omega_n)$ is exact at the limit of an infinite dimensional system, or inifinite coordination number, provided that the hopping matrix is scaled with dimension so as to keep the kinetic energy scale of the system comparable to the interaction strength.

For completeness, let us compare the real-space DMFT formulation above to the original formulation of DMFT for translation invariant systems. If the system under consideration is translation invariant and its solution is assumed to be uniform, it is advantageous to rewrite the DMFT equations in the momentum space. This is the original formulation of DMFT. In the momentum space the local self-energy becomes is independent of momentum, and thus, the approximation is given by $\mathbf{\Sigma}(\mathbf{k}, i\omega_n) = \mathbf{\Sigma}(i\omega_n)$, while the whole lattice Dyson equation is

$$\boldsymbol{G}(\mathbf{k}, i\omega_n) = [\boldsymbol{G}_0^{-1}(\mathbf{k}, i\omega_n) - \mathbf{\Sigma}(i\omega_n)]^{-1}. \tag{5.12}$$

The local Green's function is now the same at every lattice site, and obtained as the inverse Fourier transformation of the lattice Green's function

$$\boldsymbol{G}_{\mathrm{local}}(i\omega_n) = \boldsymbol{G}_{ii}(i\omega_n) = \sum_{\mathbf{k}} \boldsymbol{G}(\mathbf{k}, i\omega_n). \tag{5.13}$$

Finally, the bath Green's function of the impurity problem is of the same form as above

$$\boldsymbol{\mathcal{G}}^{-1}_{\mathrm{Bath}}(i\omega_n) = [\boldsymbol{G}_{\mathrm{local}}(i\omega_n)]^{-1} + \mathbf{\Sigma}(i\omega_n) \tag{5.14}$$

Thus, in the translation invariant case, there is only one impurity problem to solve instead of one for each lattice site as in real-space DMFT.[3] Typically, a change of variables from momentum to energy is made in Equation (5.13) leading to an integration over the density of states.

In Publication III a chain variant of the real-space DMFT method was incorporated to study the dimensional crossover of a spin-polarized Fermi gas. In this approach, the real-space formalism was used in one spatial dimension, while in the other two dimensions the system was assumed translation invariant. Thus, in the transverse dimensions, it was possible

[3]Note that the size of the real-space problem can also be reduced if the lattice and the external potential have symmetries in common, e.g. mirror symmetry.

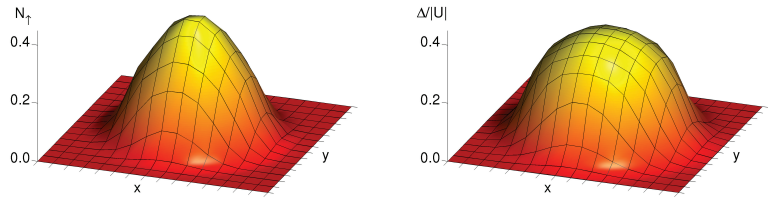

Figure 5.3. Real-space DMFT can describe non-uniform systems such as quantum gases in a trap. In this example case, we have computed the density and order parameter profiles of a balanced two-component Fermi gas in the BCS state in a 2D lattice with 16×16 lattice sites and a spherically symmetric harmonic trapping potential. Here, $N_\uparrow$ is the density of up spins (here $N_\uparrow = N_\downarrow$) and Δ denotes the order parameter.

to recast the lattice problem as an integration over the transverse momentum. The benefit of this approach was that it facilitated the study of large traps containing a Fermi gas with a shell structure of multiple different phases.

The trapped, attractively interacting two-component Fermi gas in an optical lattice of 1D chains which are coupled to form an anisotropic cubic lattice is described by the following Hubbard Hamiltonian

$$\begin{aligned} H = &- t_\parallel \sum_{il\sigma} (c^\dagger_{il\sigma} c_{(i+1)l\sigma} + \text{h.c.}) - t_\perp \sum_{\langle ll' \rangle} \sum_{i\sigma} c^\dagger_{il\sigma} c_{il'\sigma} \\ &+ U \sum_{il} \hat{n}_{il\uparrow} \hat{n}_{il\downarrow} + \sum_{il\sigma} (V_i - \mu_\sigma) \hat{n}_{il\sigma}. \end{aligned} \tag{5.15}$$

Here, the hopping within a single 1D chain is denoted by $t_\parallel$, and these chains are connected in the transverse direction by the hopping $t_\perp$. If $t_\perp = 0$ the system consists of independent 1D chains, whereas the case $t_\parallel = t_\perp$ corresponds to a 3D cubic lattice. In the region $0 < t_\perp < t_\parallel$ the model describes a crossover between 1D and 3D geometries. The indices l and i denote the 1D chain and the lattice site within the 1D chain, respectively. We consider a harmonic potential $V_i = \omega_\parallel^2 i^2/2$ along the chains with the trap frequency $\omega_\parallel$.

To formulate the DMFT method for this model, we assume again that the self-energy of the system is site diagonal, *i.e.* $\boldsymbol{\Sigma}_{ii';ll'}(i\omega_n) = \delta_{i,i'}\delta_{l,l'}\boldsymbol{\Sigma}_{i;l}(i\omega_n)$. On the assumption that the system is homogeneous in the interchain direction, the self-energy is independent of the chain index l, and as a result the Nambu Green's function of the system is of the following form

$$[\boldsymbol{G}^{-1}(\boldsymbol{k}_\perp; i\omega_n)]_{ij} = [\boldsymbol{G}^0_\parallel(i\omega_n)]^{-1}_{ij} - [\epsilon_{\boldsymbol{k}_\perp} \boldsymbol{\sigma}_3 + \boldsymbol{\Sigma}_i(i\omega_n)]\delta_{ij}. \tag{5.16}$$

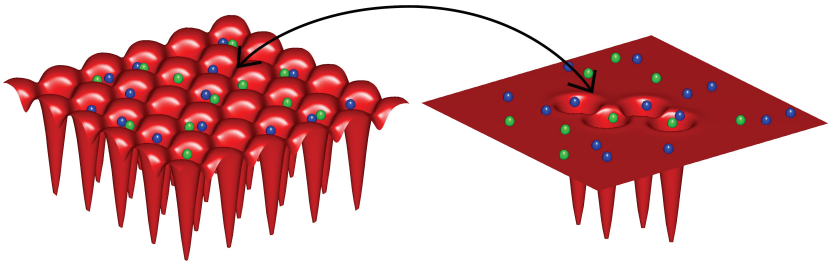

Figure 5.4. In cluster DMFT methods the impurity problem contains more than one interacting lattice site, enabling the study of non-local quantum fluctuations.

Above, $\boldsymbol{G}^0_{\parallel}$ is the non-interacting Nambu Green's function for a 1D chain and $\boldsymbol{\sigma}$ is the Pauli matrix. We have the notation $\epsilon_{\boldsymbol{k}_\perp}$ for the transverse kinetic term $\epsilon_{\boldsymbol{k}_\perp} \equiv -2t_\perp(\cos k_x + \cos k_y)$ where $\boldsymbol{k}_\perp = (k_x, k_y)$ is the transverse quasi-momentum. The equation above is obtained by starting from the standard real-space formulation of the Dyson equation and by taking the Fourier transformation in the transverse position space. In this notation, the bath Green's function of the DMFT calculations is given as

$$[\boldsymbol{\mathcal{G}}_{\mathrm{Bath},i}(i\omega_n)]^{-1} = [\sum_{\boldsymbol{k}_\perp} \boldsymbol{G}_{ii}(\boldsymbol{k}_\perp; i\omega_n)]^{-1} + \boldsymbol{\Sigma}_i(i\omega_n). \tag{5.17}$$

We discuss the results obtained in this model in Section 5.4 together with the results of the cluster DMFT calculations.

5.2 Cluster DMFT

Cluster DMFT is a generic name for a group of methods which aim for a systematic improvement of the DMFT method by the inclusion of non-local quantum fluctuations, i.e. including more terms to the self-energy than just the local one [106]. As illustrated in Figure 5.4, in these methods the impurity problem is no more a single site problem, but instead a cluster of several interacting lattice sites. Typically, these methods converge to the exact result when the cluster size grows to infinity.

There are several different variants of cluster DMFT, and arguably the most widespread ones are cellular dynamical mean field theory (CDMFT) and dynamical cluster approximation (DCA). Of these methods, CDMFT corresponds to the idea of defining the cluster on the real-space lattice, whereas DCA can be characterized as a coarse graining in the momentum space. Nonetheless, both methods lead to a formally similar impurity problem. The cluster selection of the CDMFT method breaks the transla-

tion invariance of the original lattice, while DCA is specifically laid out to enforce the translation invariance.

In Publication V there were two physical aspects of the problem, which motivated an approach different from either of the alternatives above to the formulation of the cluster DMFT problem. In this work the cluster approximation was constructed by defining a 1D chain with a periodic boundary condition as the cluster, and forming the bath in the transverse 2D plane. Firstly, in Publication V our interest was directed at the quasi-1D regime of the anisotropic Hubbard model, which motivates the choice of the 1D chain as the cluster [107, 108, 109]. Secondly, one of our objectives in Publication V was to describe the superfluid state in the most general form possible, i.e. allowing also the description of systems with spontaneously broken spatial translation invariance, in particular the FFLO state. Now, the need to describe such spatially non-uniform solutions rendered a DCA based approach with enforced translation invariance undesirable. On the other hand, in CDMFT the translation invariance is in effect broken by construction, and this may exaggerate the stability of spatially non-uniform solutions. The virtue of the periodic boundary condition for the cluster is precisely that it allows for solutions with broken translation invariance without an explicit bias in their favor. With the notations introduced in Section 5.1, the self-energy of this model is defined as

$$\boldsymbol{\Sigma}_{ii';ll'}(i\omega_n) = \delta_{l,l'}\boldsymbol{\Sigma}_{ii';l}(i\omega_n), \tag{5.18}$$

i.e. the self-energy is block diagonal in the interchain index l, while all the indices i and i' run through all the self-energy terms, both local and non-local, within the 1D chain. Since we again consider the system and all physical quantities as homogeneous in the interchain direction, the self-energy is independent of the chain index l. Thus, the Green's function of the system can be written as

$$[\boldsymbol{G}(\boldsymbol{k}_\perp; i\omega_n)]^{-1}_{ij} = [\boldsymbol{G}^0_\parallel(i\omega_n)]^{-1}_{ij} - \epsilon_{\boldsymbol{k}_\perp}\boldsymbol{\sigma}_3\delta_{ij} - \boldsymbol{\Sigma}_{ij}(i\omega_n) \tag{5.19}$$

in which $\boldsymbol{G}^0_\parallel$ is the non-interacting Green's function of a single chain, and $\epsilon_{\boldsymbol{k}_\perp}$ is the transverse kinetic energy defined as $\epsilon_{\boldsymbol{k}_\perp} \equiv -2t_\perp(\cos k_x + \cos k_y)$ with the transverse quasi-momentum $\boldsymbol{k}_\perp = (k_x, k_y)$. The bath Green's function of the DMFT calculations is then given by

$$[\boldsymbol{\mathcal{G}}_{\mathrm{Bath}}(i\omega_n)]^{-1}_{ij} = \left[\sum_{\boldsymbol{k}_\perp} \boldsymbol{G}(\boldsymbol{k}_\perp; i\omega_n)\right]^{-1}_{ij} + \boldsymbol{\Sigma}_{ij}(i\omega_n). \tag{5.20}$$

Again, the bath Green's function together with the interaction strength defines the impurity problem of this cluster DMFT formulation. Also in the case of the cluster problem, the physical solution is the fixed point of this mapping, and is found by an iteration in which the impurity problem is repeatedly solved, and the self-energy given by it fed back to form the next bath Green's function. In the following section we will take a closer look at how this impurity problem can be solved.

5.3 Continuous-time auxiliary-field quantum Monte Carlo

Markov chain Monte Carlo (MCMC) is a class of methods which produce a sample $\{X_i\}_{i=1}^N$ from a given probability distribution $p(X)$ via the construction of a Markov chain whose equilibrium distribution is $p(X)$. A Markov chain is a discrete-time stochastic process without memory, and can be characterized by the transition probabilities $w(X, Y)$ from configuration X to configuration Y. The Markov Chain converges to its equilibrium distribution, assumed as above $p(X)$, if it is ergodic and satisfies the balance condition. Here, ergodicity means that it is possible to reach every configuration in a finite number of steps and without a periodic cycle, while the balance condition is given by

$$\int p(X)w(X, Y)\, dX = p(Y). \tag{5.21}$$

In most MCMC schemes the balance condition is replaced with the more strict detailed balance condition, which is given by

$$p(X)w(X, Y) = p(Y)w(Y, X). \tag{5.22}$$

Arguably, the most common way to implement the MCMC method is the Metropolis-Hastings algorithm. In the Metropolis-Hastings algorithm, the idea is to divide the transition from X to Y to two parts: proposing the configuration Y with probability $w^p(X, Y)$ and accepting Y as the next configuration of the chain with probability $w^a(X, Y)$ so that $w(X, Y) = w^p(X, Y)w^a(X, Y)$. The acceptance probability is defined as

$$w^a(X, Y) = \min\left(1, \frac{p(Y)w^p(Y, X)}{p(X)w^p(X, Y)}\right), \tag{5.23}$$

while the proposal probability $w^p(X, Y)$ is specific to the implementation and fixed by the rule chosen for forming the candidate configuration Y. The term $p(Y)w^p(Y, X)/(p(X)w^p(X, Y))$ is called the acceptance ratio. Notice that to produce the sample $\{X_i\}_{i=1}^N$ by means of this algorithm, only

ratios of probabilities are required, and therefore, the distribution $p(X)$ need not be normalized.

In general, the sample $\{X_i\}_{i=1}^N$ can be utilized further for a number of different applications, but in the context of this section, the most relevant of these is the evaluation of the expected value of an observable $M(X)$ with respect to the probability distribution $p(X)$ as follows

$$\boldsymbol{E}[M] = \int M(X)p(X)\,dX = \frac{1}{N}\sum_{i=1}^{N} M(X_i) + \mathcal{O}\left(\frac{1}{\sqrt{N}}\right) \tag{5.24}$$

The equation above can also be interpreted as the numerical evaluation of a definite integral. Here, it is notable that the convergence rate of the numerical estimate $1/\sqrt{N}$ does not depend on the dimension of the integral, which is the case for deterministic quadratures. Hence, the Monte Carlo method is the preferred choice over deterministic quadratures for high-dimensional integrals.

The basic idea of quantum Monte Carlo (QMC) methods is to re-express the quantum problem at hand as a multidimensional integral where the integrand is weighted by a probability measure, and then, to apply the Markov chain Monte Carlo method to the problem. Quite commonly, this involves mapping the quantum partition function Z to a classical probability distribution defined on a set of configurations X

$$Z = \mathrm{Tr}\{\exp(-\beta H)\} = \sum_X p(X), \tag{5.25}$$

and finding a form for the observables of interest, such as the Green's function, in terms of this probability distribution

$$G = \sum_X G(X)p(X). \tag{5.26}$$

An example of such a mapping would be to express the Hamiltonian H in matrix form and diagonalize it, in which case the configurations X would simply correspond to the eigenstates of H, and $p(X)$ would be the Boltzmann weight calculated from the eigenenergy of the state. However, this particular mapping is viable in practice only for very small systems, as the size of the Hilbert space scales exponentially with e.g. the particle number. On the other hand, we know from experience that if this route can be taken, there is no need to perform any Monte Carlo sampling to compute the observables. Therefore, the central question is if a *computationally efficient* mapping can be found. To give a glimpse of how broad this question is, we point out that there is no reason for the configurations

X to be physically meaningful objects such as individual quantum states, any possible way the chop up the quantum partition function into computationally tractable pieces is allowed. Moreover, it is perfectly reasonable to look into approximate mappings and not only exact representations of the partition function.

It turns out that while such computationally viable mappings have been conceived, there is no single universal solution to this question. Instead, there are many different types of quantum Monte Carlo algorithms available to us for different physical systems, depending for instance on whether we are dealing with bosons or fermions, or with continuum or lattice. Moreover, there can be several different methods available for the same physical system, in which case the choice of method could depend for instance on the scaling of the computational cost with respect to a control parameter of interest.

In the following, we will focus on a particular QMC method, the continuous-time auxiliary-field algorithm (CT-AUX), which is suitable for the types of impurity problems the DMFT method outlined above calls for us to solve, i.e. interacting fermions on a lattice in the presence of a bath [110]. We give here the formulae in Nambu formalism, which contains the anomalous bath Green's function $\mathcal{F}$ and thus can incorporate a superfluid symmetry breaking [111].

Consider now a cluster impurity model with total the Hamiltonian

$$H = H_0 + H_U. \tag{5.27}$$

Here H_U is the Hubbard interaction term defined on N_c cluster sites shifted by a density type term to accommodate later manipulations

$$H_U = U \sum_{i=1}^{N_c} [n_{i\uparrow} n_{i\downarrow} - \frac{1}{2}(n_{i\uparrow} + n_{i\downarrow} - 1)], \tag{5.28}$$

and H_0 represents the non-interacting part of the system with a corresponding shift.

In the CT-AUX method the partition function is written as follows

$$Z = \sum_{k=0}^{\infty} \sum_{s_1,\ldots,s_k=\pm 1} \sum_{r_1,\ldots,r_k}^{N_c} \int_0^\beta d\tau_1 \cdots \int_{\tau_{k-1}}^\beta d\tau_k \left(\frac{K}{2\beta N_c}\right)^k e^{-\gamma \sum s_i} Z_0 Z_k(X_k). \tag{5.29}$$

Here the vector X_k is a shorthand notation for all the variables of summation and integration at order k, $X = \{s_1, \tau_1, r_1, s_2, \tau_2, r_2, \ldots, s_k, \tau_k, r_k\}$ where s_i, r_i and τ_i are the auxiliary field, cluster site and complex time,

respectively. Here, $Z_0 = \mathrm{Tr}\{\exp(-\beta H_0)\}$ and the function $Z_k(X_k)$ is defined as a determinant

$$Z_k(X) = \det(\boldsymbol{N}_k^{-1}), \tag{5.30}$$

where N_k is a $2k \times 2k$-matrix with defined as

$$\boldsymbol{N}_k^{-1} = \boldsymbol{\Gamma} - g(\boldsymbol{\Gamma} - \boldsymbol{I}). \tag{5.31}$$

Above, $\boldsymbol{I}$ is the identity matrix, and $\boldsymbol{\Gamma}$ and and g are $k \times k$ matrices of 2×2 Nambu blocks, which are defined as follows.

$$\begin{aligned}
\boldsymbol{\Gamma}_{ij} &= \delta_{ij} e^{\gamma s_i} \begin{bmatrix} 1 & 0 \\ 0 & 1 \end{bmatrix}, \\
\boldsymbol{g}_{ij} &= \begin{bmatrix} \mathcal{G}_{r_i r_j \uparrow}(\tau_i - \tau_j) & \mathcal{F}_{r_i r_j}(\tau_i - \tau_j) \\ -\mathcal{F}^*_{r_i r_j}(\tau_i - \tau_j) & \mathcal{G}_{r_j r_i \downarrow}(\tau_j - \tau_i) \end{bmatrix}.
\end{aligned} \tag{5.32}$$

The Green's functions appearing above are the components of the 2×2 Nambu bath Green's function. Note that the Bath-subscript has been left out for clarity and that we follow here the typical QMC sign convention of the Green's function, $\mathcal{G}_{r_i r_i \uparrow}(0^+) \geq 0$. Now, let us try to clarify the content of Equation (5.29). In this equation the partition function is expanded in the interaction picture as a series with respect to $H_U + K/\beta$ where K is a positive constant. The series in k and multiple integrals over τ are a result of this expansion. Now, the auxiliary field s (often called spin) is a result of decoupling the interaction term with a Hubbard-Stratonovich transformation

$$H_U + K/\beta = \frac{K}{2\beta N_c} \sum_{i, s_i = \pm 1} e^{\gamma s_i (n_{i\uparrow} + n_{i\downarrow} - 1)}, \tag{5.33}$$

where $\gamma = \cosh^{-1}\left(1 - \frac{\beta U}{2K}\right)$. The determinant form (5.30) can then be derived by using the standard machinery of determinantal Monte Carlo introduced originally in the context of the Blankenbecler-Scalapino-Sugar and Hirsch-Fye algorithms.

The observables, i.e. the Nambu Green's functions can be expressed similarly to the partition function as a summation over the auxiliary field, cluster index and integration over complex time. We illustrate this for the $\boldsymbol{G}_{rr'\uparrow}$ Green's function which has the expression

$$\begin{aligned}
\boldsymbol{G}_{rr'\uparrow}(\tau, \tau') = & \frac{1}{Z} \sum_{k=0}^{\infty} \sum_{s_1, \ldots, s_k = \pm 1} \sum_{r_1, \ldots, r_k}^{N_c} \int_0^\beta d\tau_1 \cdots \int_{\tau_{k-1}}^\beta d\tau_k \\
& \left(\frac{K}{2\beta}\right)^k e^{-\gamma \sum s_i} Z_0 Z_k(X_k) \boldsymbol{G}_{rr'\uparrow}(\tau, \tau', X_k).
\end{aligned} \tag{5.34}$$

Here, the Green's function of a single configuration X_k is

$$\boldsymbol{G}_{rr'\uparrow}(\tau,\tau',X_k) = \boldsymbol{\mathcal{G}}_{rr'\uparrow}(\tau,\tau') - \boldsymbol{R}_k(r,\tau)\boldsymbol{N}_k\boldsymbol{Q}_k(r',\tau'). \tag{5.35}$$

Here, $\boldsymbol{R}_k(r,\tau)$ is a row vector consisting of k Nambu blocks whereas $\boldsymbol{Q}_k(r',\tau')$ is the corresponding column vector, and their components are

$$\begin{aligned}\boldsymbol{R}_i(r,\tau) &= (e^{(\gamma s_i)}-1)[\mathcal{G}_{rr_i}(\tau,\tau_i)\ \mathcal{F}_{rr_i}(\tau,\tau_i)],\\ \boldsymbol{Q}_j(r',\tau') &= [-\mathcal{G}_{r_jr'}(\tau_j,\tau')\ \mathcal{F}^\dagger_{r_jr'}(\tau_j,\tau')]^T.\end{aligned} \tag{5.36}$$

In the numerics, it is preferrable to use the following Fourier transformation of the measurement formula

$$\boldsymbol{G}_{rr'\uparrow}(i\omega_n,X_k) = \boldsymbol{\mathcal{G}}_{rr'\uparrow}(i\omega_n) - \boldsymbol{R}_k(r,i\omega_n)\boldsymbol{N}_k(i\omega_n)\boldsymbol{Q}_k(r',i\omega_n), \tag{5.37}$$

where $\boldsymbol{Q}_k$ and $\boldsymbol{R}_k$ contain now the Green's functions evaluated at the indicated Matsubara frequency and $\boldsymbol{N}_k(i\omega_n)$ is defined in each Nambu block as

$$\{\boldsymbol{N}_k(i\omega_n)\}_{pq} = e^{i\omega_n\tau_p}\{\boldsymbol{N}_k\}_{pq}e^{-i\omega_n\tau_q}. \tag{5.38}$$

There are two main benefits one obtains by the frequency space measurement. Firstly, the DMFT self-consistency equation is written in Matsubara frequency space, so the result is eventually needed in this form. Secondly, the numerical noise is reduced in the frequency space measurement, since the term containing the QMC matrix $\boldsymbol{N}_k$ is multiplied by two Green's functions proportional to $1/i\omega_n$ at high frequencies, where the numerical noise is typically the most severe. Notice also that the instantaneous Green's function of the QMC simulation is not physical, and in particular, not time-translation invariant. Time translation invariance would be restored only in the Monte Carlo average. However, in frequency space it is possible to exploit the fact that the bath is time translation invariant and measure only the part of the Green's function which is diagonal in frequency (i.e. the physical part).

Now, we may outline how the formalism above is utilized in the MCMC sampling. Equation (5.34) is the expected value (or multidimensional integral) of $\boldsymbol{G}_{rr'\uparrow}(X_k)$ with the remaining expression giving the probability density for the configurations X_k. Possible updates of X_k would be to remove from or add to the configuration a point (s_i,τ_i,r_i), or alternately to flip one of the auxiliary spins while keeping the configuration otherwise the same. The crucial trick behind the whole algorithm is that the non-trivial part of the computation of the acceptance ratios is the computation of ratios of two determinants, which only differ by one row and

column vector (or a $2 \times 2k$ matrix in the Nambu formulation). Utilizing standard formulae for determinants of block matrices, this calculation is reduced to a simple vector-matrix-vector multiplication, making the sampling tremendously more efficient. In the case of the spin-flip acceptance ratio, a further simplification to a 2×2 determinant occurs. Similar manipulations can also be used to recompute the matrix N_k, if an update is accepted. The Green's function is then measured at given intervals following Equation (5.37).

The total computational cost of the algorithm scales as $(\beta U N_C)^3$, essentially since the average expansion order $\langle k \rangle$ (and average matrix size) scales with $\beta U N_C$. For large problems the performance of the algorithm can be improved by optimizing its cache usage with delayed spin-flip update [112] and submatrix update [113] techniques.

An important benefit of the CT-AUX algorithm is that it is formally exact, and the only error in the result is that of Monte Carlo sampling. This can be compared to the earlier determinantal Monte Carlo methods such as the Hirsch-Fye algorithm, which involves a discretization of the complex time. In fact, the emphasis on the continuous time in the name of the method originates from this improvement. Another benefit of the CT-AUX algorithm is its reasonable scaling with cluster size. The cubic scaling of CT-AUX can be contrasted e.g. with the exponential scaling of the continuous-time hybridization expansion solver (CT-HYB) [110]. It needs to be pointed out though, that in multi-orbital problems the scaling comparison of these two algorithms favors the CT-HYB algorithm.

5.4 Spin-polarized superfluidity in real-space DMFT and cluster DMFT calculations

Now, let us turn to the DMFT based results about spin-polarized superfluidity in the 1D-3D dimensional crossover. Consider first the real-space DMFT model for the trapped system presented in Publication III. In the calculations, we used the trap frequency of $\omega_{\parallel} = 1.1 \times 10^{-2}$. The spin-populations were controlled with the choice of the chemical potentials so that the total particle number was held approximately constant while varying the polarization $P = (N_\uparrow - N_\downarrow)/(N_\uparrow + N_\downarrow)$. The interaction strength U was chosen for each value of the transverse hopping $t_\perp$ such that it corresponded to the lattice equivalent of the unitarity limit [114].

Figure 5.5 demonstrates the main findings of this study. The FFLO

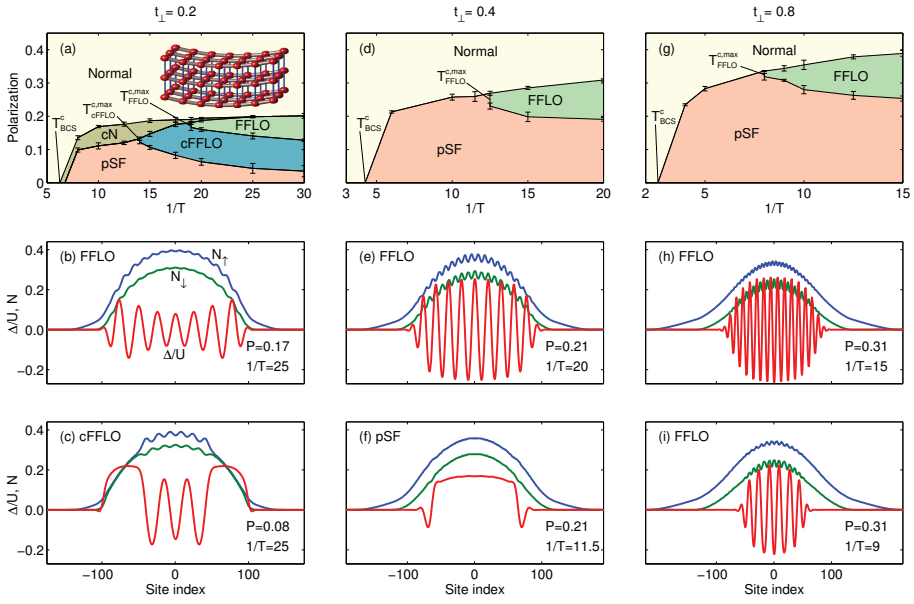

Figure 5.5. The phase diagram of a trapped, spin-polarized Fermi gas in a 1D-3D dimensional crossover as predicted by the real-space DMFT method. The inset of panel (a) depicts the geometry of the system. The label pSF refers to a polarized superfluid phase. In the cN shell structure there is a normal state at the center of the trap with a superfluid state towards the edges. In the cFFLO shell structure we have FFLO in the middle and superfluid at the edges. The polarization is defined as $P = (N_\uparrow - N_\downarrow)/(N_\uparrow + N_\downarrow)$. Panel (a) contains the phase diagram for quasi-1D lattice with $t_\perp = 0.2$, and in panels (b) and (c) we have an example of the FFLO and the cFFLO. In panel (d) we have the phase diagram for $t_\perp = 0.4$. Panels (e) and (f) compare the FFLO and the polarized superfluid phases at constant polarization for $t_\perp = 0.4$. The phase diagram in quasi-3D geometry with $t_\perp = 0.8$ is given in (g) Panels (h) and (i) demonstrate how the FFLO state is affected by the increasing temperature. All energies and temperatures are in units of $t_\parallel = 1$. Figure originally published in Publication III.

state is stable in a broad parameter region throughout the dimensional crossover. In the quasi-1D geometry, the FFLO state appears first at the trap center when temperature is lowered. For larger transverse hopping strength the system demonstrates a 3D-like behavior, and the FFLO instability appears first at the trap edges. This behavior is reflected also in the fact that in 3D-like systems the amplitude maximum of the order parameter is at the trap center, whereas in the quasi-1D regime it resides close to cloud edge. At zero temperature the polarized superfluid region would be fully paired with zero spin polarization. However, at finite temperatures also the conventional BCS superfluid can accommodate a non-zero polarization. This can be thought of as having the population imbalance in the thermal excitations of the BCS state. Now, the experimental control parameter is the total polarization of the system. The previous argument means that at finite temperatures the polarized superfluid region in the shell structure reduces the size of the FFLO region, since a part of the spin-imbalance reuquired to drive the FFLO mechanism is redistributed to the polarized superfluid (pSF) region. In Publication III we also showed that at turning point between 1D-like and 3D-like behavior, at $t_\perp = 0.3t_\parallel$, the FFLO order parameter demonstrates a behavior particularly amenable to experimental probes: The amplitude of the order parameter remains uniform over several oscillation periods despite the harmonic confinement and variation of the density profile.

We then turn to study the role of the non-local quantum fluctuations. This was the central question studied in Publication V and the main results of this study are summarized by the phase diagram of Figure 5.6. The very first observation is that the BCS transition temperature as predicted by cluster DMFT decreases monotonously towards the 1D-limit. This is drastically different from the critical temperature given by the single-site DMFT method which remains roughly constant over the parameter range of Figure 5.6. Now, one can immediately deduce that the behavior of the cluster DMFT result can not be accounted for by single particle effects, i.e. the changes to the non-interacting density of states brought on by the dimensionality – these effects would also be visible in the single-site DMFT results. A further investigation of the self-energy of the system as a function of the dimensionality confirms that indeed the rapid decline of superfluidity at the 1D limit is caused by the non-local quantum fluctuations, for details see Publication V.

Judging by their crucial impact on the BCS physics, one might antic-

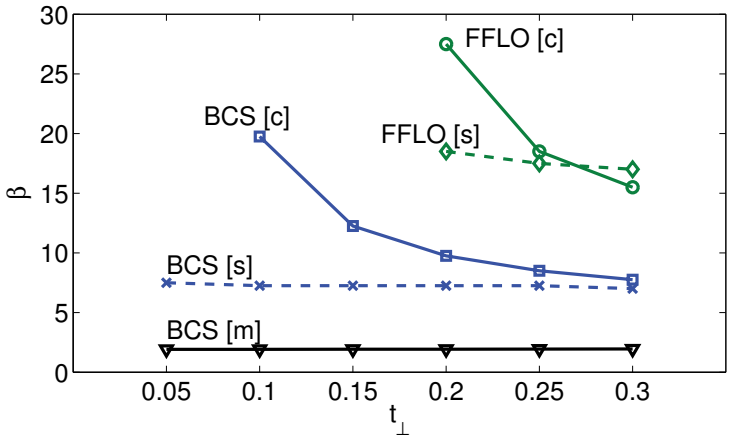

Figure 5.6. The phase diagram of the attractive Hubbard model with strong lattice anisotropy. Here the system is at half-filling with the interaction strength $U = -3$. The solid line with square marks gives the BCS critical temperature for the balanced system at half-filling as predicted by cluster DMFT [c], while the dashed line with crosses is the single-site DMFT result [s]. The prediction of the static mean-field method [m] is also given for comparison, and is plotted with the black line with triangles. The FFLO critical temperature is found by varying the polarization of the system at a given temperature while maintaining the total density at half-filling. The cluster size is $N_c = 36$ at and above $t_\perp = 0.15$. At $t_\perp = 0.1$ a cluster of $N_c = 42$ lattice sites is needed to have good convergence. The BCS transition becomes computationally too expensive to study below $t_\perp = 0.1$ because of the decreasing temperature combined with the increase in cluster size required for convergence. With the FFLO transition, this limit is reached below $t_\perp = 0.2$. Figure adapted from Publication V.

ipate that the non-local quantum fluctuations would be able to destroy entirely the delicate spatial structure of the FFLO state. It turns out, on the contrary, that when the system is subjected to spin-polarization the oscillating order parameter and density profile of the FFLO state prevail over the spatially uniform pairing. However, there is a correction to the critical temperature, and for instance at $t_\perp = 0.2$ the cluster model predicts a reduction of the critical temperature by a factor of 0.67 in comparison to single-site calculations. At the FFLO critical temperature, the polarization of the system varies from $P = 3\ \%$ at $t_\perp = 0.2$ to $P = 5\ \%$ at $t_\perp = 0.3$ in the cluster model whereas the single-site model predicts a polarization of $P = 6\ \%$ in the corresponding parameter region. A further noteworthy result of Publication V is that the oscillatory FFLO-structure dominates the self-energy of the system at all frequencies, which in turn suggests that the FFLO character of the state is very robust and experimentally discernible even when non-local quantum fluctuations are taken into account.

6. Conclusions

The application of a spin-dependent potential to a Josephson junction or an analogous physical system leads to Josephson oscillations at the same frequency but with different amplitudes – the spin-asymmetric Josephson effect. The phenomenon is explained by a careful breakdown of the Josephson tunneling to elementary processes and the subsequent identification of an interference contribution from intermediate states of broken Cooper pairs. This previously unnoticed interference term is significant also in the conventional Josephson effect, leading to the conclusion that the conventional view of the Josephson effect as the tunneling of bosonic Cooper pairs is inadequate. In the context of quantum gases, the spin-asymmetric Josephson effect could be realized in a spin-dependent double well or superlattice, or possibly utilizing radio frequency pulses to couple two superfluids.

The Fulde-Ferrell-Larkin-Ovchinnikov state is a result of the interplay of spin-polarization and Cooper pairing. The state is characterized by a spatially non-uniform, anisotropic order parameter which leads to a directionally dependent density response, and in particular, anisotropic speed of sound. Our real-space DMFT studies of the FFLO state in a 1D-3D dimensional crossover suggest that the phase is stable in a broad region of parameters and that the mean field predictions concerning the shell structure of FFLO, polarized superfluid and normal phases are qualitatively speaking reasonable. The FFLO state is strong enough to survive even at the presence of non-local quantum fluctuations as indicated by our cluster DMFT investigations, though the non-local fluctuations do lower the critical temperature of the state.

Bibliography

[1] I. Bloch, J. Dalibard, and W. Zwerger. Many-body physics with ultracold gases. *Rev. Mod. Phys.*, 80:885, 2008.

[2] S. Giorgini, L. P. Pitaevskii, and S. Stringari. Theory of ultracold atomic Fermi gases. *Rev. Mod. Phys.*, 80:1215, 2008.

[3] W. Ketterle and M.W. Zwierlein. Making, probing and understanding ultracold Fermi gases. *Riv. Nuovo Cimento*, 31:247, 2008.

[4] C. Chin, R. Grimm, P. Julienne, and E. Tiesinga. Feshbach resonances in ultracold gases. *Rev. Mod. Phys.*, 82:1225, 2010.

[5] I. Bloch. Ultracold quantum gases in optical lattices. *Nat. Phys.*, 1:23, 2005.

[6] F. Schwabl. *Advanced Quantum Mechanics*. Springer-Verlag Berlin Heidelberg, 2005.

[7] L. E. Ballentine. *Quantum mechanics: A Modern development*. World Scientific, 1998.

[8] H. J. Lipkin. *Quantum Mechanics: New Approaches to Selected Topics*. North-Holland Publishing Coompany (Amsterdam), 1973.

[9] A. L. Migdall, J. V. Prodan, W. D. Phillips, T. H. Bergeman, and H. J. Metcalf. First Observation of Magnetically Trapped Neutral Atoms. *Phys. Rev. Lett.*, 54:2596, 1985.

[10] E. L. Raab, M. Prentiss, A. Cable, S. Chu, and D. E. Pritchard. Trapping of Neutral Sodium Atoms with Radiation Pressure. *Phys. Rev. Lett.*, 59:2631, 1987.

[11] H. J. Metcalf and P. van der Straten. *Laser Cooling and Trapping of Neutral Atoms*. Wiley-VCH, 2004.

[12] W. Ketterle and N. J. van Druten. Evaporative cooling of trapped atoms. *Adv. At. Mol. Opt. Phys.*, 37:181, 1996.

[13] C. J Pethick and H. Smith. *Bose-Einstein condensation in dilute gases*. Cambridge university press, 2002.

[14] M. W. Zwierlein, A. Schirotzek, C. H. Schunck, and W. Ketterle. Fermionic Superfluidity with Imbalanced Spin Populations. *Science*, 311:492, 2006.

[15] G. B. Partridge, W. Li, R. I. Kamar, Y. Liao, and R. G. Hulet. Pairing and phase separation in a polarized Fermi gas. *Science*, 311:503, 2006.

[16] M. H. Anderson, J. R. Ensher, M. R. Matthews, C. E. Wieman, and E. A. Cornell. Observation of Bose-Einstein condensation in a dilute atomic vapor. *Science*, 269:198, 1995.

[17] C. C. Bradley, C. A. Sackett, J. J. Tollett, and R. G. Hulet. Evidence of Bose-Einstein Condensation in an Atomic Gas with Attractive Interactions. *Phys. Rev. Lett.*, 75:1687, 1995.

[18] K. B. Davis, M.-O. Mewes, M. R. Andrews, N. J. van Druten, D. S. Durfee, D. M. Kurn, and W. Ketterle. Bose-Einstein Condensation in a Gas of Sodium Atoms. *Phys. Rev. Lett.*, 75:3969, 1995.

[19] M. R. Andrews, C. G. Townsend, H. J. Miesner, D. S. Durfee, D. M. Kurn, and W. Ketterle. Observation of Interference Between Two Bose Condensates. *Science*, 275:637, 1997.

[20] K. W. Madison, F. Chevy, W. Wohlleben, and J. Dalibard. Vortex Formation in a Stirred Bose-Einstein Condensate. *Phys. Rev. Lett.*, 84:8068, 2000.

[21] J. R. Abo-Shaeer, C. Raman, J. M. Vogels, and W. Ketterle. Observation of Vortex Lattices in Bose-Einstein Condensates. *Science*, 292:476, 2001.

[22] B. DeMarco and D. S. Jin. Onset of Fermi Degeneracy in a Trapped Atomic Gas. *Science*, 285:1703, 1999.

[23] C. A. Regal, M. Greiner, and D. S. Jin. Observation of Resonance Condensation of Fermionic Atom Pairs. *Phys. Rev. Lett.*, 92:040403, 2004.

[24] M. Bartenstein, A. Altmeyer, S. Riedl, S. Jochim, C. Chin, J. Hecker Denschlag, and R. Grimm. Crossover from a Molecular Bose-Einstein Condensate to a Degenerate Fermi Gas. *Phys. Rev. Lett.*, 92:120401, 2004.

[25] M. W. Zwierlein, C. A. Stan, C. H. Schunck, S. M. F. Raupach, A. J. Kerman, and W. Ketterle. Condensation of Pairs of Fermionic Atoms near a Feshbach Resonance. *Phys. Rev. Lett.*, 92:120403, 2004.

[26] T. Bourdel, L. Khaykovich, J. Cubizolles, J. Zhang, F. Chevy, M. Teichmann, L. Tarruell, S. J. J. M. F. Kokkelmans, and C. Salomon. Experimental Study of the BEC-BCS Crossover Region in Lithium 6. *Phys. Rev. Lett.*, 93:050401, 2004.

[27] C. Chin, M. Bartenstein, A. Altmeyer, S. Riedl, S. Jochim, J. H. Denschlag, and R. Grimm. Observation of the pairing gap in a strongly interacting Fermi gas. *Science*, 305:1128, 2004.

[28] G. B. Partridge, K. E. Strecker, R. I. Kamar, M. W. Jack, and R. G. Hulet. Molecular Probe of Pairing in the BEC-BCS Crossover. *Phys. Rev. Lett.*, 95:020404, 2005.

[29] M. W. Zwierlein, J. R. Abo-Shaeer, A. Schirotzek, C. H. Schunck, and W. Ketterle. Vortices and superfluidity in a strongly interacting Fermi gas. *Nature*, 435:1047, 2005.

[30] M. Taglieber, A.-C. Voigt, T. Aoki, T. W. Hänsch, and K. Dieckmann. Quantum Degenerate Two-Species Fermi-Fermi Mixture Coexisting with a Bose-Einstein Condensate. *Phys. Rev. Lett.*, 100:010401, 2008.

[31] E. Wille, F. M. Spiegelhalder, G. Kerner, D. Naik, A. Trenkwalder, G. Hendl, F. Schreck, R. Grimm, T. G. Tiecke, J. T. M. Walraven, S. J. J. M. F. Kokkelmans, E. Tiesinga, and P. S. Julienne. Exploring an Ultracold Fermi-Fermi Mixture: Interspecies Feshbach Resonances and Scattering Properties of ^{6}Li and ^{40}K. *Phys. Rev. Lett.*, 100:053201, 2008.

[32] S. Taie, Y. Takasu, S. Sugawa, R. Yamazaki, T. Tsujimoto, R. Murakami, and Y. Takahashi. Realization of a SU(2)×SU(6) System of Fermions in a Cold Atomic Gas. *Phys. Rev. Lett.*, 105:190401, 2010.

[33] A. H. Hansen, A. Y. Khramov, W. H. Dowd, A. O. Jamison, B. Plotkin-Swing, R. J. Roy, and S. Gupta. Production of quantum-degenerate mixtures of ytterbium and lithium with controllable interspecies overlap. *Phys. Rev. A*, 87:013615, 2013.

[34] M. P. A. Fisher, P. B. Weichman, G. Grinstein, and D. S. Fisher. Boson localization and the superfluid-insulator transition. *Phys. Rev. B*, 40:546, 1989.

[35] D. Jaksch, C. Bruder, J. I. Cirac, C. W. Gardiner, and P. Zoller. Cold bosonic atoms in optical lattices. *Phys. Rev. Lett.*, 81:3108, 1998.

[36] M. Greiner, O. Mandel, T. Esslinger, T. W. Hänsch, and I. Bloch. Quantum phase transition from a superfluid to a Mott insulator in a gas of ultracold atoms. *Nature*, 415:39, 2002.

[37] R. Jördens, N. Strohmaier, K. Günter, H. Moritz, and T. Esslinger. A Mott insulator of fermionic atoms in an optical lattice. *Nature*, 455:204, 2008.

[38] U. Schneider, L. Hackermüller, S. Will, T. Best, I. Bloch, T. A. Costi, R. W. Helmes, D. Rasch, and A. Rosch. Metallic and Insulating Phases of Repulsively Interacting Fermions in a 3D Optical Lattice. *Science*, 322:1520, 2008.

[39] M. Köhl, H. Moritz, T. Stöferle, K. Günter, and T. Esslinger. Fermionic Atoms in a Three Dimensional Optical Lattice: Observing Fermi Surfaces, Dynamics, and Interactions. *Phys. Rev. Lett.*, 94:080403, 2005.

[40] W. S. Bakr, J. I. Gillen, A. Peng, S. Fölling, and M. Greiner. A quantum gas microscope for detecting single atoms in a Hubbard-regime optical lattice. *Nature*, 462:74, 2009.

[41] J. F. Sherson, C. Weitenberg, M. Endres, M. Cheneau, I. Bloch, and S. Kuhr. Single-atom-resolved fluorescence imaging of an atomic Mott insulator. *Nature*, 467:68, 2010.

[42] K. Baumann, C. Guerlin, F. Brennecke, and T. Esslinger. Dicke quantum phase transition with a superfluid gas in an optical cavity. *Nature*, 464:1301, 2010.

[43] D. Greif, T. Uehlinger, G. Jotzu, L. Tarruell, and T. Esslinger. Short-Range Quantum Magnetism of Ultracold Fermions in an Optical Lattice. *Science*, 340:1307–1310, 2013.

[44] C. Becker, P. Soltan-Panahi, J. Kronjäger, S. Dörscher, K. Bongs, and K. Sengstock. Ultracold quantum gases in triangular optical lattices. *New J. Phys.*, 12:065025, 2010.

[45] L. Tarruell, D. Greif, T. Uehlinger, G. Jotzu, and T. Esslinger. Creating, moving and merging Dirac points with a Fermi gas in a tunable honeycomb lattice. *Nature*, 483:302, 2012.

[46] (Eds.) P. Törmä and K. Sengstock. *Quantum gas experiments – exploring many-body states*. Imperial College Press, 2014.

[47] T. Stöferle, H. Moritz, C. Schori, M. Köhl, and T. Esslinger. Transition from a Strongly Interacting 1D Superfluid to a Mott Insulator. *Phys. Rev. Lett.*, 92:130403, 2004.

[48] S. Trotzky, Y.-A. Chen, U. Schnorrberger, P. Cheinet, and I. Bloch. Controlling and Detecting Spin Correlations of Ultracold Atoms in Optical Lattices. *Phys. Rev. Lett.*, 105:265303, 2010.

[49] M. Lewenstein, A. Sanpera, and V. Ahufinger. *Ultracold Atoms in Optical Lattices: Simulating quantum many-body systems*. Oxford University Press, 2012.

[50] Masahito Ueda. *Fundamentals and new frontiers of Bose-Einstein condensation*. World Scientific, 2010.

[51] S. R. White. Density matrix formulation for quantum renormalization groups. *Phys. Rev. Lett.*, 69:2863, 1992.

[52] G. Vidal. Efficient Simulation of One-Dimensional Quantum Many-Body Systems. *Phys. Rev. Lett.*, 93:040502, 2004.

[53] (Eds.) C. Miniatura, L.-C. Kwek, M. Ducloy, B. Grémaud, and B.-G. Englert. *Ultracold Gases and Quantum Information: Lecture Notes of the Les Houches Summer School in Singapore: Volume 91, July 2009*. Oxford University Press, 2011.

[54] A. J. Leggett. *Quantum liquids: Bose condensation and Cooper pairing in condensed-matter systems*, volume 34. Oxford University Press, 2006.

[55] H. Deng, H. Haug, and Y. Yamamoto. Exciton-polariton Bose-Einstein condensation. *Rev. Mod. Phys.*, 82:1489, 2010.

[56] D. J. Dean and M. Hjorth-Jensen. Pairing in nuclear systems: from neutron stars to finite nuclei. *Rev. Mod. Phys.*, 75:607, 2003.

[57] J. Bardeen, L. N. Cooper, and J. R. Schrieffer. Theory of Superconductivity. *Phys. Rev.*, 108:1175, 1957.

[58] A. M. Clogston. Upper limit for the critical field in hard superconductors. *Phys. Rev. Lett.*, 9:266, 1962.

[59] B. S. Chandrasekhar. A note on the maximum critical field of high-field superconductors. *Appl. Phys. Lett.*, 1:7, 1962.

[60] P. Fulde and R. A. Ferrell. Superconductivity in a Strong Spin-Exchange Field. *Phys. Rev.*, 135:A550, 1964.

[61] A. I. Larkin and Yu. N. Ovchinnikov. Inhomogeneous state of superconductors. *Zh. Eksp. Teor. Fiz.*, 47:1136, 1964.

[62] A. I. Larkin and Yu. N. Ovchinnikov. Inhomogeneous state of superconductors. *Soviet Physics – JETP*, 20:762, 1965.

[63] C. Qu, Z. Zheng, M. Gong, Y. Xu, L. Mao, X. Zou, G. Guo, and C. Zhang. Topological superfluids with finite-momentum pairing and Majorana fermions. *Nat. comm.*, 4:2710, 2013.

[64] W. Zhang and W. Yi. Topological Fulde–Ferrell–Larkin–Ovchinnikov states in spin–orbit-coupled Fermi gases. *Nat. comm.*, 4:2711, 2013.

[65] H. A. Radovan, N. A. Fortune, T. P. Murphy, S. T. Hannahs, E. C. Palm, S. W. Tozer, and D. Hall. Magnetic enhancement of superconductivity from electron spin domains. *Nature*, 425:51, 2003.

[66] A. Bianchi, R. Movshovich, C. Capan, P. G. Pagliuso, and J. L. Sarrao. Possible Fulde-Ferrell-Larkin-Ovchinnikov Superconducting State in $CeCoIn_5$. *Phys. Rev. Lett.*, 91:187004, 2003.

[67] K. Kumagai, M. Saitoh, T. Oyaizu, Y. Furukawa, S. Takashima, M. Nohara, H. Takagi, and Y. Matsuda. Fulde-Ferrell-Larkin-Ovchinnikov State in a Perpendicular Field of Quasi-Two-Dimensional $CeCoIn_5$. *Phys. Rev. Lett.*, 97:227002, 2006.

[68] V. F. Correa, T. P. Murphy, C. Martin, K. M. Purcell, E. C. Palm, G. M. Schmiedeshoff, J. C. Cooley, and S. W. Tozer. Magnetic-Field-Induced Lattice Anomaly inside the Superconducting State of $CeCoIn_5$: Anisotropic Evidence of the Possible Fulde-Ferrell-Larkin-Ovchinnikov State. *Phys. Rev. Lett.*, 98:087001, 2007.

[69] R. Lortz, Y. Wang, A. Demuer, P. H. M. Böttger, B. Bergk, G. Zwicknagl, Y. Nakazawa, and J. Wosnitza. Calorimetric Evidence for a Fulde-Ferrell-Larkin-Ovchinnikov Superconducting State in the Layered Organic Superconductor κ-$(BEDT\text{-}TTF)_2Cu(NCS)_2$. *Phys. Rev. Lett.*, 99:187002, 2007.

[70] W. A. Coniglio, L. E. Winter, K. Cho, C. C. Agosta, B. Fravel, and L. K. Montgomery. Superconducting phase diagram and fflo signature in λ-$(bets)_2gacl_4$ from rf penetration depth measurements. *Phys. Rev. B*, 83:224507, 2011.

[71] Y. Liao, A. S. C. Rittner, T. Paprotta, W. Li, G. B. Partridge, R. G. Hulet, S.K. Baur, and E.J. Mueller. Spin-imbalance in a one-dimensional Fermi gas. *Nature*, 467:567, 2010.

[72] T. Koponen, J. Kinnunen, J. P. Martikainen, L. M. Jensen, and P. Törmä. Fermion pairing with spin-density imbalance in an optical lattice. *New J. Phys.*, 8:179, 2006.

[73] T. K. Koponen and T. Paananen and J. -P. Martikainen and P. Törmä. Finite temperature phase diagram of a polarized fermi gas in an optical lattice. *Phys. Rev. Lett.*, 99:120403, 2007.

[74] G. D. Mahan. *Many-particle Physics*. Plenum, 2000.

[75] H. Bruus and K. Flensberg. *Many-Body Quantum Theory in Condensed Matter Physics*. Oxford University Press, 2004.

[76] G. Stefanucci and R. van Leeuwen. *Nonequilibrium Many-Body Theory of Quantum Systems*. Cambridge University Press, 2013.

[77] G. Sarma. On the influence of a uniform exchange field acting on the spins of the conduction electrons in a superconductor. *J. Phys. Chem. Solids*, 24:1029, 1963.

[78] W. V. Liu and F. Wilczek. Interior Gap Superfluidity. *Phys. Rev. Lett.*, 90:047002, 2003.

[79] G. Baym and L. P. Kadanoff. Conservation Laws and Correlation Functions. *Phys. Rev.*, 124:287, 1961.

[80] G. Baym. Self-Consistent Approximations in Many-Body Systems. *Phys. Rev.*, 127:1391, 1962.

[81] P. W. Anderson. Random-Phase Approximation in the Theory of Superconductivity. *Phys. Rev.*, 112:1900, 1958.

[82] M. Tinkham. *Introduction to Superconductivity*. Courier Dover Publications, 2004.

[83] Gh.-S. Paraoanu, M. Rodriguez, and P. Törmä. Josephson effect in superfluid atomic Fermi gases. *Phys. Rev. A*, 66:041603, 2002.

[84] C. Cohen-Tannoudji, J. Dupont-Roc, and G. Grynberg. *Atom-Photon interactions*. John Wiley & Sons, 1998.

[85] B. D. Josephson. Possible new effects in superconductive tunnelling. *Phys. Lett.*, 1:251, 1962.

[86] V. Ambegaokar and A. Baratoff. Tunneling Between Superconductors. *Phys. Rev. Lett.*, 10:486, 1963.

[87] B. D. Josephson. Coupled Superconductors. *Rev. Mod. Phys.*, 36:216, 1964.

[88] F. S. Bergeret, A. F. Volkov, and K. B. Efetov. Enhancement of the Josephson Current by an Exchange Field in Superconductor-Ferromagnet Structures. *Phys. Rev. Lett.*, 86:3140, 2001.

[89] F. S. Bergeret, A. F. Volkov, and K. B. Efetov. Odd triplet superconductivity and related phenomena in superconductor-ferromagnet structures. *Rev. Mod. Phys.*, 77:1321, 2005.

[90] Y. M. Blanter and F. W. J. Hekking. Supercurrent in long SFFS junctions with antiparallel domain configuration. *Phys. Rev. B*, 69:024525, 2004.

[91] K.-H. Lee and K. J. Chang. Analytic continuation of the dynamic response function using an N-point Padé approximant. *Phys. Rev. B*, 54:R8285, 1996.

[92] J. M. Edge and N. R. Cooper. Signature of the Fulde-Ferrell-Larkin-Ovchinnikov Phase in the Collective Modes of a Trapped Ultracold Fermi Gas. *Phys. Rev. Lett.*, 103:065301, 2009.

[93] J. M. Edge and N. R. Cooper. Collective modes as a probe of imbalanced Fermi gases. *Phys. Rev. A*, 81:063606, 2010.

[94] L. Radzihovsky. Quantum liquid-crystal order in resonant atomic gases. *Phys. C (Amsterdam)*, 481:189, 2012.

[95] Z. Koinov, R. Mendoza, and M. Fortes. Rotonlike Fulde-Ferrell Collective Excitations of an Imbalanced Fermi Gas in a Two-Dimensional Optical Lattice. *Phys. Rev. Lett.*, 106:100402, 2011.

[96] R. Mendoza, M. Fortes, M. A. Solís, and Z. Koinov. Superfluidity of a spin-imbalanced Fermi gas in a three-dimensional optical lattice. *Phys. Rev. A*, 88:033606, 2013.

[97] A. Altland and B. D. Simons. *Condensed matter field theory*. Cambridge University Press, 2010.

[98] A. Georges, G. Kotliar, W. Krauth, and M. J. Rozenberg. Dynamical mean-field theory of strongly correlated fermion systems and the limit of infinite dimensions. *Rev. Mod. Phys.*, 68:13, 1996.

[99] A. Hubener, M. Snoek, and W. Hofstetter. Magnetic phases of two-component ultracold bosons in an optical lattice. *Phys. Rev. B*, 80:245109, 2009.

[100] P. Anders, E. Gull, L. Pollet, M. Troyer, and P. Werner. Dynamical mean-field theory for bosons. *New J. Phys.*, 13:075013, 2011.

[101] R. W. Helmes, T. A. Costi, and A. Rosch. Mott Transition of Fermionic Atoms in a Three-Dimensional Optical Trap. *Phys. Rev. Lett.*, 100:056403, 2008.

[102] M. Snoek, I. Titvinidze, C. Tőke, K. Byczuk, and W. Hofstetter. Antiferromagnetic order of strongly interacting fermions in a trap: real-space dynamical mean-field analysis. *New J. Phys.*, 10:093008, 2008.

[103] A. Koga, J. Bauer, P. Werner, and T. Pruschke. Polarized superfluid state in a three-dimensional fermionic optical lattice. *Physica (Amsterdam)*, 43E:697, 2011.

[104] D.-H. Kim, J. J. Kinnunen, J.-P. Martikainen, and P. Törmä. Exotic Superfluid States of Lattice Fermions in Elongated Traps. *Phys. Rev. Lett.*, 106:095301, 2011.

[105] A. Comanac. *Dynamical mean field theory of correlated electron systems: New algorithms and applications to local observables (PhD thesis)*. Columbia University, 2007.

[106] T. Maier, M. Jarrell, T. Pruschke, and M. H. Hettler. Quantum cluster theories. *Rev. Mod. Phys.*, 77:1027, 2005.

[107] A. Georges, T. Giamarchi, and N. Sandler. Interchain conductivity of coupled Luttinger liquids and organic conductors. *Phys. Rev. B*, 61:16393, 2000.

[108] S. Biermann, A. Georges, A. Lichtenstein, and T. Giamarchi. Deconfinement Transition and Luttinger to Fermi Liquid Crossover in Quasi-One-Dimensional Systems. *Phys. Rev. Lett.*, 87:276405, 2001.

[109] C. Berthod, T. Giamarchi, S. Biermann, and A. Georges. Breakup of the Fermi Surface Near the Mott Transition in Low-Dimensional Systems. *Phys. Rev. Lett.*, 97:136401, 2006.

[110] E. Gull, A. J. Millis, A. I. Lichtenstein, A. N. Rubtsov, M. Troyer, and P. Werner. Continuous-time Monte Carlo methods for quantum impurity models. *Rev. Mod. Phys.*, 83:349, 2011.

[111] A. Koga and P. Werner. Polarized Superfluidity in the Imbalanced Attractive Hubbard Model. *J. Phys. Soc. Jpn.*, 79:064401, 2010.

[112] G. Alvarez, M. S. Summers, D. E. Maxwell, M. Eisenbach, J. S. Meredith, J. M. Larkin, J. Levesque, T. A. Maier, P. R. C. Kent, E. F. D'Azevedo, and T. C. Schulthess. *in SC '08: Proceedings of the 2008 ACM/IEEE Conference on Supercomputing*. IEEE Press, Piscataway, NJ, 2008.

[113] E. Gull, P. Staar, S. Fuchs, P. Nukala, M. S. Summers, T. Pruschke, T. C. Schulthess, and T. Maier. Submatrix updates for the continuous-time auxiliary-field algorithm. *Phys. Rev. B*, 83:075122, 2011.

[114] E. Burovski, N. Prokof'ev, B. Svistunov, and M. Troyer. Critical temperature and thermodynamics of attractive fermions at unitarity. *Phys. Rev. Lett.*, 96:160402, 2006.

Aalto-DD 78/2014

ISBN 978-952-60-5708-8
ISBN 978-952-60-5709-5 (pdf)
ISSN-L 1799-4934
ISSN 1799-4934
ISSN 1799-4942 (pdf)

Aalto University
School of Science
Department of Applied Physics
www.aalto.fi

BUSINESS +
ECONOMY

ART +
DESIGN +
ARCHITECTURE

SCIENCE +
TECHNOLOGY

CROSSOVER

DOCTORAL
DISSERTATIONS